STOCHASTIC MODELING OF TRANSPORT AND DEGRADATION OF

REACTIVE SOLUTES IN HETEROGENEOUS AQUIFERS

A Thesis

by

ZIAD JOSEPH FADEL

Submitted to the Office of Graduate Studies of
Texas A&M University
in partial fulfillment of the requirements for the degree of

MASTER OF SCIENCE

May 2005

Major Subject: Civil Engineering

STOCHASTIC MODELING OF TRANSPORT AND DEGRADATION OF

REACTIVE SOLUTES IN HETEROGENEOUS AQUIFERS

A Thesis

by

ZIAD JOSEPH FADEL

Submitted to Texas A&M University
in partial fulfillment of the requirements
for the degree of

MASTER OF SCIENCE

Approved as to style and content by:

_____
Jeffrey Cunningham
(Co-Chair of Committee)

_____
Anthony Cahill
(Co-Chair of Committee)

_____
Hongbin Zhan
(Member)

_____
David Rosowsky
(Head of Department)

May 2005

Major Subject: Civil Engineering

ABSTRACT

Stochastic Modeling of Transport and Degradation of Reactive

Solutes in Heterogeneous Aquifers. (May 2005)

Ziad Joseph Fadel, B.E., American University of Beirut

Co-Chairs of Advisory Committee: Dr. Jeffrey Cunningham
Dr. Anthony Cahill

Hydraulic conductivity fields (K) and degradation rate constants (α) are commonly used in predicting the fate and transport of reactive contaminants. The natural heterogeneity in aquifer porous materials and its effect on hydrological parameters such as K and α has to be accounted for by using an appropriate stochastic approach.

The spatial distribution of K and its correlation with α were examined. Random fields of K having prescribed mean, variance, and correlation lengths were generated using the HYDRO_GEN method. Transport simulations were conducted for an ensemble of two-dimensionally heterogeneous aquifers. Both positive and negative correlations of K and α were considered.

The solute's remaining mass in both the positive and negative correlation scenarios was found to be, on average, within a small range. Concentration profiles for a positive K-α correlation displayed a more uniform behavior of the contaminated plume, compared to a more variable spreading in the negatively correlated cases.

To My Parents

ACKNOWLEDGEMENTS

TABLE OF CONTENTS

LIST OF FIGURES

FIGURE   Page

LIST OF TABLES

CHAPTER I

INTRODUCTION

Over the past three decades, groundwater contamination has become a highly active area of research in the environmental field. However, one major feature that hinders the investigation of this problem is the heterogeneity of aquifer porous materials, which typically occurs at length scales significantly smaller than the field scales of practical interest [*Gelhar*, 1993]. In an effort to overcome this limitation, several stochastic techniques have been developed to model contaminants' fate and transport under spatially variable conditions [*Dagan*, 1989; *Gelhar*, 1993]. This variability affects several hydrological properties (hydraulic conductivity, dispersion coefficient, degradation rate, etc.) as well as the major physical and biological processes that govern groundwater flow (advection, sorption, degradation, etc.).

By definition, the word "contaminant" is used to describe a chemical, biological, or radiological substance that produces an adverse effect when present in a certain environment (groundwater in this case). Only a small number of contaminants are truly inert and harmless when present in groundwater. A large variety of solutes can be dangerous to both human and environmental health, but can become less hazardous when undergoing the process of biodegradation.

———————

This thesis follows the style and format of the *Water Resources Research* Journal.

As mentioned earlier, it is a well-established fact that the hydraulic conductivity and the degradation rate are heterogeneously distributed in space. However, it has not yet been proven if these two variables are either positively or negatively correlated, and whether this correlation has any significant effect on contaminant behavior. Several applications dealing with spatial variability in aquifers and its effect on contaminants' fate and transport have been reported in the literature (e.g. correlation between the sorption's distribution coefficient K_d and the hydraulic conductivity [*Allen-King et al.*, 1998; *Robin et al.*, 1991]), whereas the connection between the hydraulic conductivity and the degradation rate remains the subject of wide speculation despite some intensive research [*Miralles-Wilhelm and Gelhar*, 1996].

The purpose of this project is to quantify how contaminant fate and transport in groundwater are affected by the correlation between two spatially-varying properties, namely, hydraulic conductivity (K) and degradation rate (α). Two sets of transport simulations were conducted along an ensemble of two-dimensionally (2-D) heterogeneous aquifers: the first set based on a positive correlation between K and α, and the second based on a negative correlation. If the simulations showed that the contaminant fate depended strongly upon the correlation, then it would be important to further investigate and research the K-α relationship. If the contaminant behavior did not vary significantly in both cases, then one need not be concerned about the K-α correlation.

A brief theoretical review is given in Chapter II. Several stochastic models used in the generation of spatially correlated random fields are presented in Chapter III. The

aquifer's stochastic configuration and investigational setup are described in Chapter IV. Experimental results are discussed in Chapter V. Finally, conclusions and recommendations are summarized in Chapter VI.

CHAPTER II

THEORETICAL BACKGROUND

In this section, the major processes that describe mass or solute transport in groundwater are presented. Before delving into the specifics of each of these processes, Darcy's Law, which is the driving force behind groundwater flow, is illustrated hereunder.

A. Darcy's Law

The movement of groundwater was well established by hydraulic principles reported in 1856 by Henry Darcy, who investigated the flow of water through beds of permeable sand [*Fetter*, 1994]. Darcy discovered one of the most important laws in hydrology. It states that the flow rate through porous media is proportional to the hydraulic head loss and inversely proportional to the length of the flow path. Darcy's law was originally derived in one dimension (Eq. 1), but since the hydraulic head is a function of the three dimensions, (x, y, z), Eq. 1 could also be expanded to cover two-dimensional (2-D) and three-dimensional (3-D) groundwater concerns (Eq. 2).

$$q = \frac{Q}{A} = -K\frac{dh}{dx} \tag{1}$$

$$\vec{q} = -\underline{\underline{K}}\,\nabla\,\vec{h} \tag{2}$$

where Q is the volumetric flow rate [L^3/T]; A is the cross-sectional area through which water flows [L^2]; K is the aquifer's hydraulic conductivity [L/T]; ∇h is the hydraulic gradient [L/L]; q is defined as the specific discharge (Darcy's velocity) [L/T].

B. Transport Processes

The starting point in modeling transport in porous materials is by developing partial differential equations (PDE) that describe the flux of contaminants into and out of a certain fixed volume within the aquifer, also known as the representative elementary volume (REV) [*Bear*, 1972]. This flux is illustrated by the following mass balance equation:

$$
\begin{Bmatrix} \text{Rate of} \\ \text{Change of} \\ \text{Solute's} \\ \text{Mass within} \\ \text{the REV} \end{Bmatrix} = \begin{Bmatrix} \text{Inward} \\ \text{Flux of} \\ \text{Solute} \end{Bmatrix} - \begin{Bmatrix} \text{Outward} \\ \text{Flux of} \\ \text{Solute} \end{Bmatrix} \pm \begin{Bmatrix} \text{Gain/Loss} \\ \text{of Solute} \\ \text{Mass Due} \\ \text{to Reactions} \end{Bmatrix} \quad (3)
$$

The two main physical processes that control the solute flux in and out of the REV are *advection* and *dispersion*. Some other mechanisms, such as *sorption* (adsorption / absorption), also play a role (retardation) in the transport of contaminants, but are disregarded in this work for illustration purposes.

1. Advection

Advection is the component of contaminant movement due to the groundwater flow. The rate of transport of the dissolved solids is equal to the average water velocity "v" in the aquifer's pores,

$$v = \frac{q}{n} \tag{4}$$

where q is the specific discharge (Eq. 1) and n the effective porosity.

Advection is sometimes referred to as "convection" in cases where groundwater flow is driven by thermal gradients. The advective flux J_{adv} [M/L^{2}T] is given by:

$$J_{adv} = nvC \tag{5}$$

where C is the solute's concentration [M/L^3]. The one-dimensional (1-D) advective transport equation is:

$$\frac{\partial C(x,t)}{\partial t} = -v_x \frac{\partial C(x,t)}{\partial x} \tag{6}$$

which describes the movement of a solute due to the process of advection only.

2. Dispersion

When the solute tends to spread out of the path that it would be expected to follow according to the advective hydraulics, the solute's concentration usually decreases. This spreading phenomenon is known as hydrodynamic dispersion, which involves two simultaneous processes: molecular diffusion and mechanical dispersion.

2.1 Molecular Diffusion

Molecular diffusion occurs at a molecular scale (smaller than the REV scale). It only affects the overall dispersion process at low groundwater velocities. It is mainly due to the thermal kinetic energy of the contaminant's molecules. The diffusion coefficient D^* is given by [*Bear*, 1972]:

$$D^* = \frac{D_m}{\tau} \tag{7}$$

where D_m is the molecular diffusivity [L^2/T]; τ is the tortuosity coefficient, which is a measure of the effect of the flow path followed by water molecules in porous media. If L is the straight-line distance between both ends of a tortuous flow path of length L_e, then τ = L_e / L (τ is always larger than 1).

2.2   Mechanical Dispersion

Mechanical dispersion takes place at an REV scale and is caused by the following three mechanisms (Figure 1): (a) some pores are larger in size than others, and hence allow water traveling through these pores to move faster; (b) some of the water will move along more tortuous flow paths, which will result in longer travel times for the same linear distance; (c) water will be faced by friction along the edges of the pores, which will lead to a faster flow at the center of the pores than along the edges.
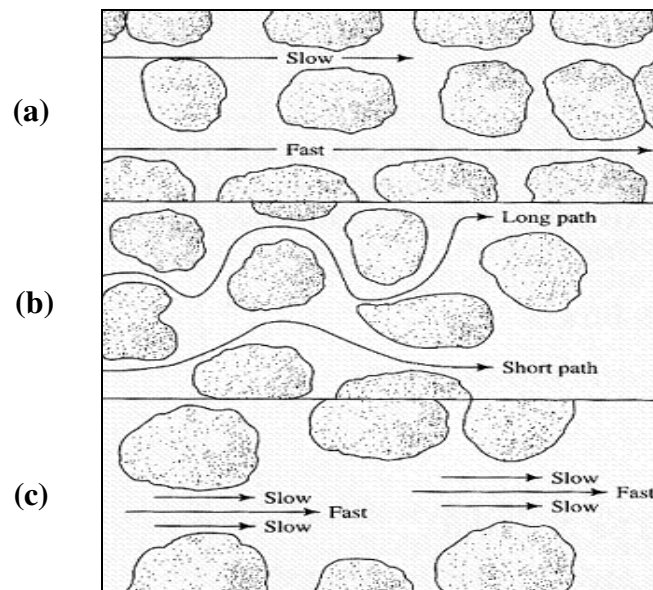
Figure 1. Factors causing mechanical dispersion [*Fetter*, 1994].

From Figure 1 above, it is clear that varying conditions across the aquifer forces groundwater to travel at different velocities. The velocity gradients lead to the mixing of the solute. The mixing that occurs along the direction of flow is called "longitudinal

dispersion", whereas the mixing taking place in the direction normal to the flow path is referred to as "transverse dispersion". In general, the former occurs to a larger degree than the latter. The longitudinal and transverse dispersion coefficients, D_m^l and D_m^t respectively, are given by:

$$D_m^l = \alpha_i v_i \tag{8}$$

$$D_m^t = \alpha_j v_i \tag{9}$$

where α_i and α_j are the dynamic dispersivities in the i (longitudinal) and j (transverse) directions [L]; v_i is the average linear velocity in the longitudinal direction [L/T]. The dispersive flux J_{disp} [M/L^{2}T] is given by:

$$J_{disp} = -nD\nabla C \tag{10}$$

where ∇C is the concentration gradient [M/L^3/L]; $D = D^* + D_m$ is the hydrodynamic dispersion coefficient [L^2/T]. The one-dimensional dispersive transport equation is:

$$\frac{\partial C(x,t)}{\partial t} = D \frac{\partial^2 C(x,t)}{\partial x^2} \tag{11}$$

which describes the movement of a solute due to the process of dispersion only.

2.3 Advective-Dispersive Equation (ADE)

For a conservative solute (non-reactive) in an isotropic homogeneous aquifer, under steady-state uniform flow, Eq. 11 and Eq. 6 can be combined with the conservation of mass principle (Eq. 3) to obtain the one-dimensional Advective-Dispersive Equation [*Bear*, 1972]:

$$n \frac{\partial C(x,t)}{\partial t} = -nv_x \frac{\partial C(x,t)}{\partial x} + nD \frac{\partial^2 C(x,t)}{\partial x^2} \tag{12}$$

3. Degradation

Also known as decay, degradation is often the most significant process resulting in the reduction of the contaminant's mass in a certain system. Decay can occur under either aerobic or anaerobic conditions, and can lead to a significant reduction in the contaminant's aqueous concentration in both cases. Several types of degradation kinetics exist in real-case groundwater applications, but the scope of this work is limited to cover first-order kinetics only.

First-order kinetics refers to a reaction process of which the reaction rate of a certain solute is proportional to the concentration of the solute itself:

$$\frac{\partial C(x,t)}{\partial t} = -\alpha C(x,t) \tag{13}$$

where C is the solute's concentration [M/L^3]; α is the reaction rate constant [$1/T$], which can also be written as $\alpha = \ln(2) / \lambda$ (λ is the solute's half-life).

Plugging Eq. 13 into Eq. 12 yields a more inclusive PDE that extends the scope of the ordinary ADE (Eq. 12) to cover degradation and 1-D transport of a reactive contaminant in porous media [*Bear*, 1972; *Bear and Verruijt*, 1987]:

$$n\frac{\partial C(x,t)}{\partial t} = -nv_x\frac{\partial C(x,t)}{\partial x} + nD\frac{\partial^2 C(x,t)}{\partial x^2} - n\alpha C(x,t) \qquad (14)$$

CHAPTER III

STOCHASTIC MODELS

As stated in the Introduction, geologic formations, which act as groundwater flow conduits, always exhibit a large degree of natural variability. It would be virtually impossible to represent some of the aquifer's soil properties using deterministic functions.

This heterogeneity usually occurs over spatial scales that are too small to be accurately reflected in a regular discretized numerical model. Hence, a stochastic approach, which accounts for this small scale variability (SSV), seems to be a more suitable solution. The idea behind such an approach is to try to include this SSV in a large scale model in order to determine its corresponding effects on groundwater flow and contaminant concentration. This process has proven to be extremely reliable, especially with the advancement of computing power, which enables researchers to analyze heterogeneous systems in great detail [*Bellin and Rubin*, 1996].

Hydraulic properties can be represented mathematically as stationary correlated space random functions (SRF). SRFs are usually characterized by their first two statistical moments: the mean and the variance [*Gelhar and Axness*, 1983]. Also, correlation length scales are needed to define or relate the structural variation in different directions along the flow domain of interest.

Some of the most widely used stochastic methods for generating correlated random fields are discussed in the following sections.

A. Mejia and Rodriguez-Iturbe (MRI) Model

As in all the stochastic models that will be reviewed in subsequent sections, this model is based on the assumption that the statistical characteristics (mean, variance, etc.) of the random field in question are known. The model uses these pre-defined statistics to simulate different realizations while preserving all of these characteristics.

The MRI model [*Mejia and Rodriguez-Iturbe*, 1974], also known as the multidimensional spectral method, represents the simulated field as a series of cosine functions having the same amplitude:

$$Z_s(x) = \sigma \left(\frac{2}{N} \right)^{1/2} \sum_{k=1}^{N} \cos \left(w_k x + \phi_k \right) \tag{15}$$

where the subscript "s" on Z_s represents the simulated realizations of the field; σ^2 is the variance of the process; ϕ_k is a random angle uniformly distributed between 0 and 2π; w_k is an independent random vector; N is the number of harmonics.

B. Matrix Decomposition Method (MDM)

This method generates normally distributed random fields having a known covariance structure, as shown in Eq. 16:

$$Z \quad = \quad We \tag{16}$$

where Z is a column vector containing the simulated values; W is a vector of weighting factors; "e" is a white noise vector having a unit variance and a zero mean.

The covariance matrix of the process, C, is obtained as the expectation of the product of Z and its transpose Z^T. C can also be computed using:

$$C = WW^T \tag{17}$$

Using the theoretical covariance value of C, W is calculated by decomposition and is then plugged into Eq. 16 to generate the field. This method generates ergodic, stationary, and isotropic fields with a rather high degree of accuracy. However, its main disadvantage is the lengthy computational time it requires, which is also a reflection of the large computer storage needed to handle matrix operations. The MDM has been proven to be highly efficient when dealing with relatively small fields [*Mantoglou and Wilson*, 1982].

C. Turning Bands Method (TBM)

The TBM was first introduced by Matheron in 1973 at the Ecole des Mines de Paris [*Matheron*, 1973]. It has been mostly used in the simulation of 3-D fields in mining applications. The originality of this technique lies in the fact that it transforms a 2-D or

3-D problem into a unidimensional (1-D) one. The TBM simulator generates single or multiple replicates of a certain stationary random process Z(x), having a user-supplied mean, variance, and correlation structure.

One of the major assumptions that underline this process is that all the replicated values are 2nd order stationary, isotropic, have a zero mean, and are normally distributed along the field $\Re^n$. If P is the region in $\Re^n$ where a 2-D or 3-D field is to be simulated, lines are generated randomly at an arbitrary origin O, as shown in Figure 2.
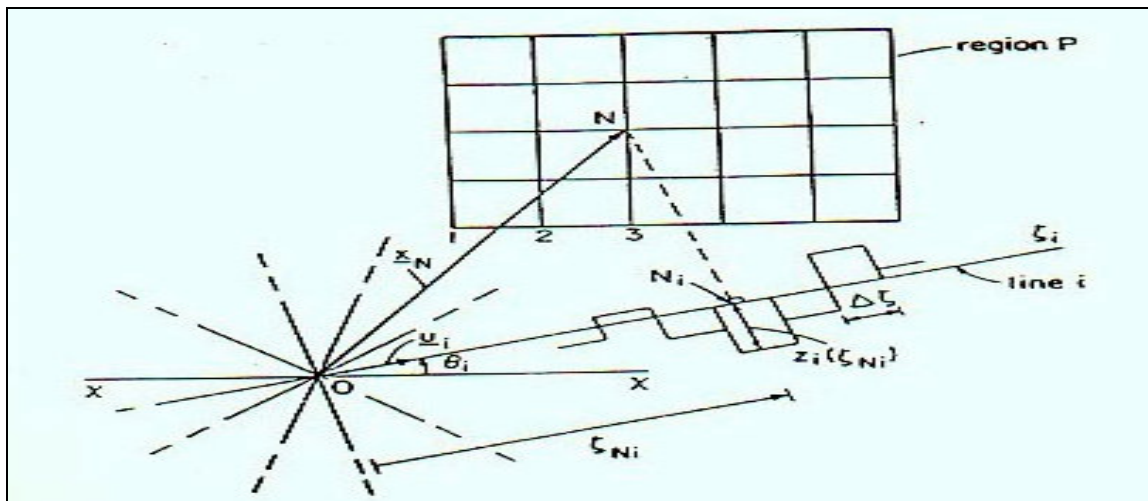
Figure 2. Schematic representation of the field P and the turning bands lines [*Mantoglou and Wilson*, 1982].

Each line "i" forms an angle θ with the X-axis. In the 2-D case shown above, since the X-axis is assumed to be fixed, the randomness of the direction of line "i" indicates that θ is uniformly distributed between 0 and 2π. As stated earlier, a 2nd order stationary 1-D process is generated with zero mean and a covariance function $C_1(\xi)$, where ξ is the coordinate along line "i". There are several forms of covariance functions

(Spherical, Exponential, Gaussian, Bessel, etc.), but the exponential $C_1(\xi)$ is most often used for reasons that are not relevant to the scope of this study. The resulting synthetic value Z_N at a certain point N is given by:

$$Z_s(x_N) = \frac{1}{\sqrt{L}} \sum_{i=1}^{L} Z_i(x_N \cdot u_i) \qquad (18)$$

where $\mathbf{x}_N$ is the location vector of point N; u_i is the unit vector along line "i"; L is the total number of lines; the inner product $(x_N.u_i)$ represents the orthogonal projection of point N onto line "i".

Although considered as one of the most accurate and efficient techniques for generating spatially correlated random fields, some of the statistical characteristics of the TBM simulated fields can be different than the theoretical values that were pre-set by the user. Such errors may be greatly reduced or even eliminated with an appropriate choice of the model parameters (covariance type, number of lines, etc.).

D. HYDRO_GEN Method

The three models discussed above, among others, have been frequently used by researchers and scientists to generate spatially correlated random fields, and the validity of these methods has been widely reported in the literature. However, the HYDRO_GEN

method (HGM) [*Bellin and Rubin*, 1996] was used in this work to generate hydraulic conductivity fields for the reasons illustrated hereunder.

The two main factors that come into play when selecting a certain stochastic approach, is its ability to reproduce the prescribed spatial moments as well as the associated computational time, which increases at a higher-than-linear rate with the dimensions of the simulated field. Another feature that directly affects the required computational effort is the accuracy of the resulting output values and their divergence from the pre-set theoretical statistical characteristics. Bellin and Rubin developed and presented the relatively new HYDRO_GEN approach (1996), and have demonstrated that the two aforementioned objectives have been largely met [*Bellin and Rubin*, 1996].

The relative ease with which the HYDRO_GEN code was compiled and its free-of-charge availability were also encouraging factors in selecting the HGM over other stochastic models.

1. General Approach

The synthetic field Z(x), which is generally a continuous function, is generated using the HYDRO_GEN algorithm, coupled with a Monte Carlo approach, over a pre-defined arbitrary grid (Figure 3). All the replicates generated by the HGM, although different in parameter magnitude, have to meet the same condition of honoring the prescribed spatial statistics (mean and variance).
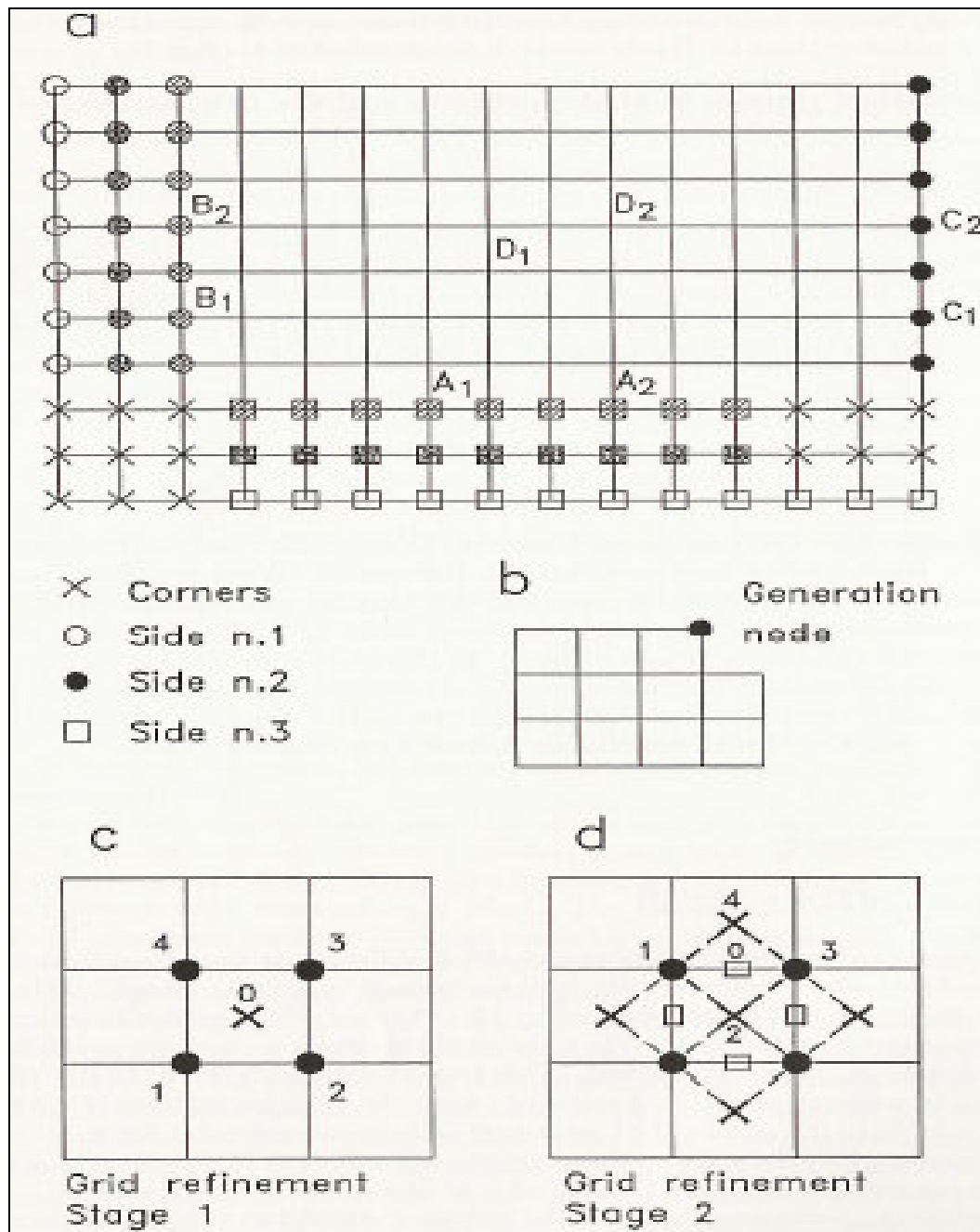
Figure 3. Domain discretization and grid refinement; a) coarse grid generation; b) search neighborhood; c) first stage refinement; d) second stage refinement [*Bellin and Rubin*, 1996].

2. Field Generation Technique

This section explains the simulation process of a normally (Gaussian) or log-normally distributed Z field. The first realization $Z(x_o)$, at a certain location x_o, is produced using a standard Gaussian random generator with an a-priori set (unconditional) mean $\mu_z(x)$ and variance $\sigma_z^2(x)$ as target statistics. Once $Z(x_o)$ is generated, it will be used as a reference when computing the Z values at adjacent nodes. In other words, the simulated value $Z(x_1)$ at a neighboring node will be conditioned on the previously generated $Z(x_o)$, using the Gaussian conditioning procedure [*Mood and Graybill*, 1963]. For a more general case, a realization $Z(x_N)$ is dependent upon the previously generated (N-1) data points, and is hence called a "conditional realization". The conditional mean, also referred to as the expected value, $<Z(x_N)>$, is given by (superscript "c" denotes "conditional"):

$$\left\langle Z^c(x_N)\right\rangle = \mu_z(x_N) + \sum_{j=1}^{N-1} \lambda_j(x_N)\left[Z(x_j) - \mu_z(x_j)\right] \tag{19}$$

The conditional variance is given by:

$$\sigma_z^{2,c}(x_N) = \sigma_z^2 - \sum_{j=1}^{N-1} \lambda_j(x_N)C_z(x_N, x_j) \tag{20}$$

where C_z is the function's covariance; the interpolation coefficients, λ_j, are the solution to the following linear system [*Dagan*, 1989]:

$$\sum_{j=1}^{N-1} \lambda_j(x_N)C_z(x_j,x_q) = C_z(x_N,x_q) \ \textit{for} \ q = 1 \rightarrow (N-1) \tag{21}$$

Once the two statistical characteristics in Eq. 19 and Eq. 20 have been calculated, the same steps used for the generic $Z(x_N)$ are also applied to compute the Z values at all designated nodes within the domain. However, one noticeable difference in the successive steps is in the growing number of previously-computed data points used for conditioning, which increases the total number of interpolation coefficients. The repetitive solving of Eq. 21 to obtain the λ_j values is considerably the most demanding aspect of the model as far as time is concerned. In order to help alleviate the computational burden, the conditioning part in the calculation of $Z(x_N)$ is based only on a limited search neighborhood of surrounding nodes, rather than on all the cells within the grid. That leads to the interpolation coefficients being computed only once for the entire domain, and hence reducing significantly the total amount of time necessary to generate the random field. The size of the search neighborhood was determined based on extensive numerical experimentation [*Bellin and Rubin*, 1996]. A step-by-step outline of the HGM can be summarized as follows:

(i). $<Z(x_N)>$ and $\sigma_z^2(x)$, required in the conditioning process of all data points in the L-shaped search neighborhood (Figure 1b – x_N placed in the upper right corner), are computed using Eq. 19 and Eq. 20.

(ii).   A realization $Z(x_N)$ is generated using the conditional mean and variance computed in (i) as target statistics.

(iii). $Z(x_N)$ is added to the database used for the conditioning at the next node (N+1) to compute $Z(x_{N+1})$.

(iv).   Same steps (i), (ii), and (iii) are repeated for the next node according to a certain pre-determined scheme.

Step (iv) above is ultimately what defines the HYDRO_GEN model and separates it from other stochastic techniques. While other methods follow random paths to generate $Z(x)$ for different realizations, the HGM applies a fixed pattern of filling in values along the domain (row-by-row or column-by-column). This regularity has proven to be very economical from a computational point of view, especially for the generation of a large number of replicates.

3. Multi-Stage Grid Refinement (MSGR)

Another factor that plays an important role in the eventual computational power needed is the grid density of the domain in question (Figure 3). Although a high density grid entails a higher computational load, it is often necessary to better mimic the true

state of the dependent variables in the actual field under investigation. For example, a high level of discretization of the hydraulic conductivity field is required in order to accurately simulate the contaminant fate and transport in a highly heterogeneous geologic formation [*Tompson and Gelhar*, 1990]. The HGM, by using the MSGR technique, takes advantage of the fact that high resolution is only needed in the domain areas where the contaminated plume has actually traveled.

The first part of the grid refinement consists of generating realizations of Z at every cell of an initially coarse grid using the four-step procedure outlined in the previous subsection. Then, the density of nodes is increased by refining subsections of the grid and Z values are generated at the additional nodes created. An example of the MSGR process is clearly illustrated in Figure 3: a realization of Z is first generated at the center of the node (Figure 3c) and is conditioned by the four neighboring cells marked with a large black dot ●; Figure 3d represents the second stage of the refinement procedure, where Z values are generated on the cell edges marked by □; this is achieved by conditioning every cell □ ("0") on its four closest cells ("1", "2", "3" and "4"), symmetrically located around the node in question.

Two HGM simulated hydraulic conductivity fields, having two different types of covariance, are illustrated in Figures 4 and 5.
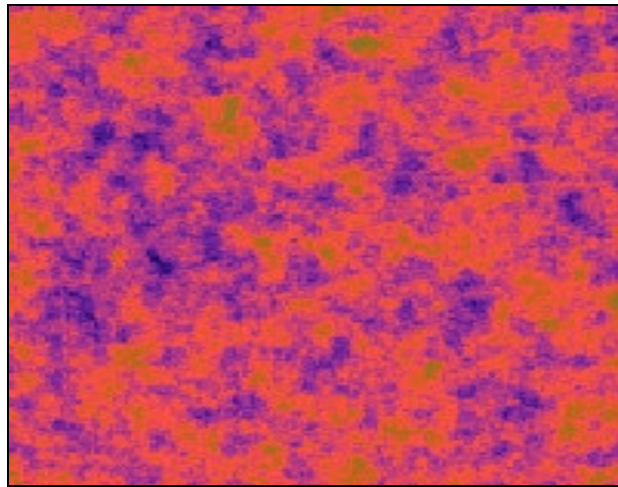
Figure 4. Hydraulic conductivity field, with an exponential covariance, generated using the HGM [*Bellin and Rubin*, 1996].
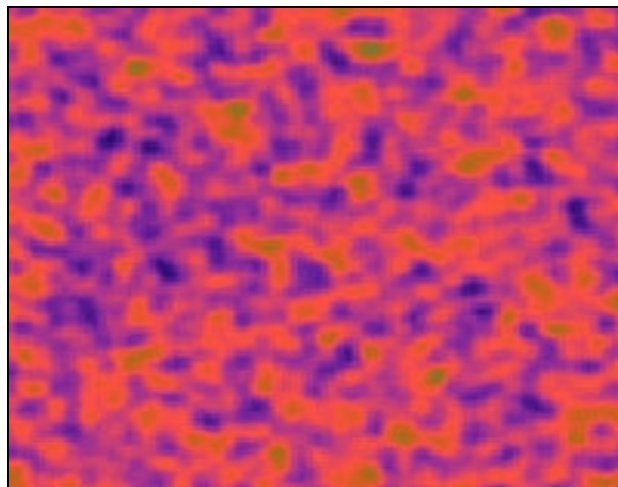
Figure 5. Hydraulic conductivity field, with a Gaussian covariance, generated using the HGM [*Bellin and Rubin*, 1996].

CHAPTER IV

APPROACH

As mentioned earlier, the natural heterogeneity and spatial variability of any hydrologic or geologic system, due to cost constraints and other limiting factors, cannot be completely modeled using deterministic methods. The use of stochastic models to overcome these limitations has proven to be a highly favored alternative. In this research, the HGM was applied to generate log-normally distributed hydraulic conductivity fields, which were used to compute the hydraulic head values at all locations within the domain. Generated heterogeneous fields of α, correlated to the random fields of K, were then integrated in the simulations of contaminant transport and degradation. All of these steps are discussed in more detail in the following sections.

A. Generation of Hydraulic Conductivity Fields

Since this research project was not based on any existing real-case groundwater aquifer, a set of assumptions was made in order to define the various parameters of the system, which can be grouped into two major categories: the input data used to describe the field properties (length, discretization, correlation lengths, mean, variance, etc.) are classified as physical parameters; the input data that are necessary to run the HYDRO_GEN algorithm are referred to as the parametric parameters. It should be noted

that most of these parameters often overlap, since they can be part of both of these categories.

Table 1 below lists all the physical parameters that define the aquifer's properties:

Table 1. Physical Parameters of the Aquifer Under Investigation.

Length in X Direction, L_x, m	Length in Y Direction, L_y, m	Porosity, n	Head at Left Boundary, H_l, m	Head at Right Boundary, H_r, m	Longitudinal Dispersion Coefficient, D_x, m^2/d	Transverse Dispersion Coefficient, D_y, m^2/d
100	10	1/3	5	4	0.3	0.03

It has been assumed that the hydraulic head at the domain's right boundary was lower than the head at the left boundary by 1 m ($h_r = h_l – 1 = 4$ m). This leads, based on Eq. 1 and Eq. 2 (Darcy's Law), to the groundwater flow being directed from the left side towards the right side, due to a hydraulic head gradient ∇h.

The first step of the HYDRO_GEN algorithm, as indicated in the previous section, would be the discretization of the domain under investigation. Figure 6 illustrates the discretized (100m x 10m) aquifer, where the hydraulic conductivity values will be determined at the center of each of the square nodes.
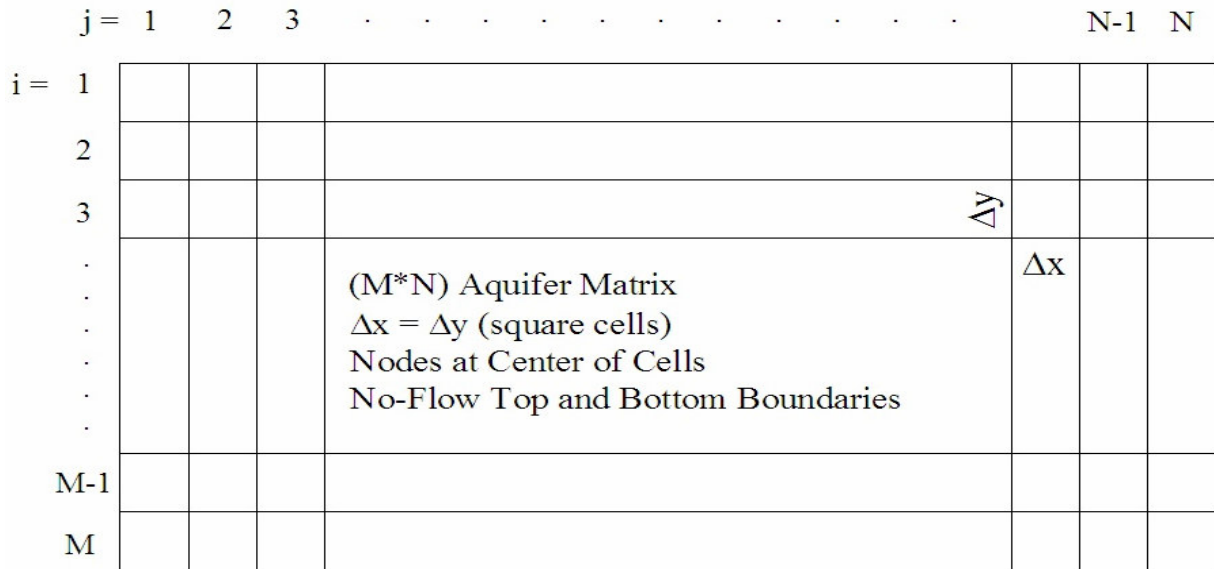
Figure 6. Discretization of the (100m x 10m) aquifer.

The parametric parameters needed to run the HYDRO_GEN algorithm are listed

in Table 2 hereunder:

Table 2. Parametric Parameters Used by the HYDRO_GEN Algorithm in the Generation of Hydraulic Conductivity Fields.

Distribution	Covariance	ln (K)		Δx,	Δy,	Correlation Length (CL)	
		Mean	Variance	m	m	CL_X, m	CL_Y, m
Log-Normal	Exponential	0	1	0.5	0.5	4	1

The chosen value of the ln (K) variance ($\sigma^2 = 1$) is reasonable based on known

field values reported in the literature [*Sudicky*, 1986; *Benson et al.*, 2000; *Garabedian et*

al., 1991].

Using a FORTRAN compiler, all the system's parameters presented in Tables 1 and 2 were incorporated into the HYDRO_GEN program in order to generate 50 different Monte Carlo replicates.

Table 3. Output Spatial Statistics of the 50 Monte Carlo Replicates Generated Using the HYDRO_GEN Method.

Replicate	ln (K)		Replicate	ln (K)	
	Mean	Variance		Mean	Variance
1	0.128414	0.839476	26	-0.03979	0.95788
2	0.163651	0.68781	27	-0.06239	0.83001
3	-0.03189	0.867376	28	-0.03889	0.997585
4	0.034259	0.902259	29	-0.34027	0.977377
5	-0.10418	0.790973	30	0.060985	0.898631
6	-0.06095	0.786962	31	-0.23119	0.938943
7	-0.01348	0.851853	32	0.106056	0.954563
8	-0.10633	0.832353	33	0.079477	0.755779
9	-0.00473	0.813863	34	-0.04036	0.994598
10	-0.02792	1.038833	35	0.1808	0.839521
11	0.312707	0.76656	36	0.079229	0.932827
12	0.106332	0.908501	37	-0.15885	0.879352
13	0.04577	0.890279	38	0.043125	0.808185
14	0.114071	0.86932	39	0.099483	0.713717
15	-0.17769	0.9087	40	-0.16014	0.89419
16	-0.01255	0.793176	41	0.132075	0.877269
17	-0.11534	0.935596	42	-0.26354	0.851676
18	-0.01028	0.952371	43	0.014207	0.817272
19	-0.01712	0.790439	44	0.077948	0.958962
20	0.073252	0.993436	45	0.066212	0.837534
21	0.081756	0.94073	46	-0.02995	0.904536
22	-0.02743	0.946001	47	-0.12287	0.853727
23	0.061265	0.97015	48	-0.06713	0.914805
24	-0.05796	0.881404	49	0.041115	0.916901
25	-0.06032	0.993533	50	0.162709	0.959363

All the 50 Monte Carlo realizations were subjected, as part of the HGM requirements, to the same prescribed spatial moments (zero mean and unit variance). The small divergence from these two a-priori set characteristics (refer to Table 3) was only due to an expected modeling error, but was always within an acceptable confidence interval [*Bellin and Rubin*, 1996].
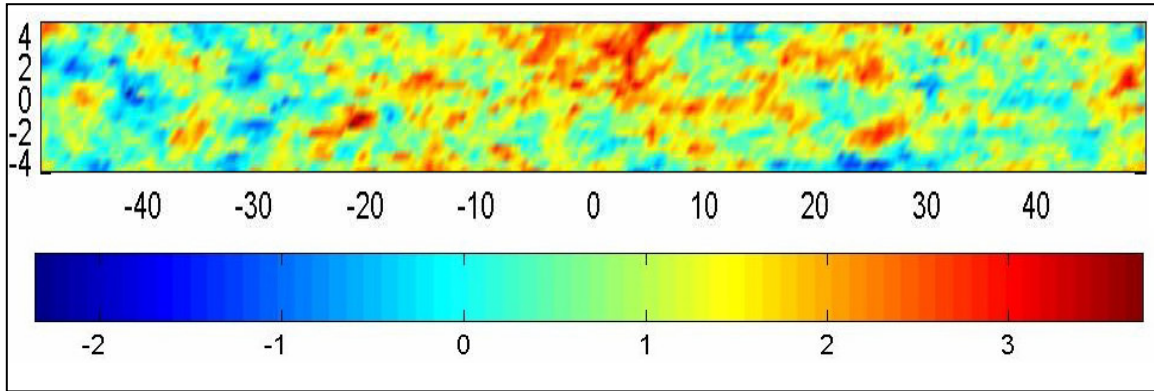
Figure 7. Contour plot of a (100m x 10m) normally distributed field, ln(K), using the parameters listed in Tables 1 and 2 (replicate 42).

The 50 normally distributed replicates were then transformed into log-normally distributed hydraulic conductivity fields, K, by taking the antilog at each grid cell:

$$K = e^{\ln(K)} \tag{22}$$

Figure 8 represents the same simulated field as in Figure 7 (normal distribution), which became log-normally distributed after being coupled with Eq. 22.
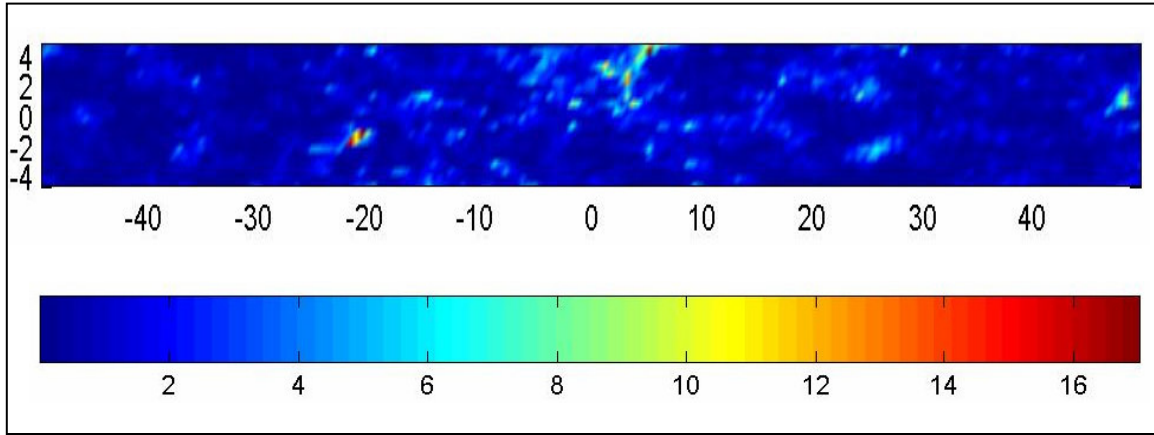
Figure 8. Contour plot of a (100m x 10m) log-normally distributed, K [m/d], using the parameters listed in Tables 1 and 2 (replicate 42).

B. Hydraulic Head

Each of the cells in the discretized domain (Figure 6) is described, at its center, by a hydraulic conductivity "K", hydraulic head "h", and a flow velocity "v" (Figure 9). While the "K" values were generated using the HGM, the Finite Volume Method (FVM) was adopted to obtain the hydraulic head at every node:

$$h_{i,j} = \frac{K_A h_{i-1,j} + K_B h_{i,j+1} + K_C h_{i+1,j} + K_D h_{i,j-1}}{K_A + K_B + K_C + K_D} \tag{23}$$

where K_A, K_B, K_C and K_D (Eq. 24) represent the harmonic mean of the hydraulic conductivities related to the groundwater flow across two adjacent cells.

$$K_A = \cfrac{2}{\left(\cfrac{1}{K_{i-1,j}} + \cfrac{1}{K_{i,j}}\right)} \;; K_B = \cfrac{2}{\left(\cfrac{1}{K_{i,j+1}} + \cfrac{1}{K_{i,j}}\right)}$$

$$K_C = \cfrac{2}{\left(\cfrac{1}{K_{i+1,j}} + \cfrac{1}{K_{i,j}}\right)} \;; K_D = \cfrac{2}{\left(\cfrac{1}{K_{i,j-1}} + \cfrac{1}{K_{i,j}}\right)}$$

(24)
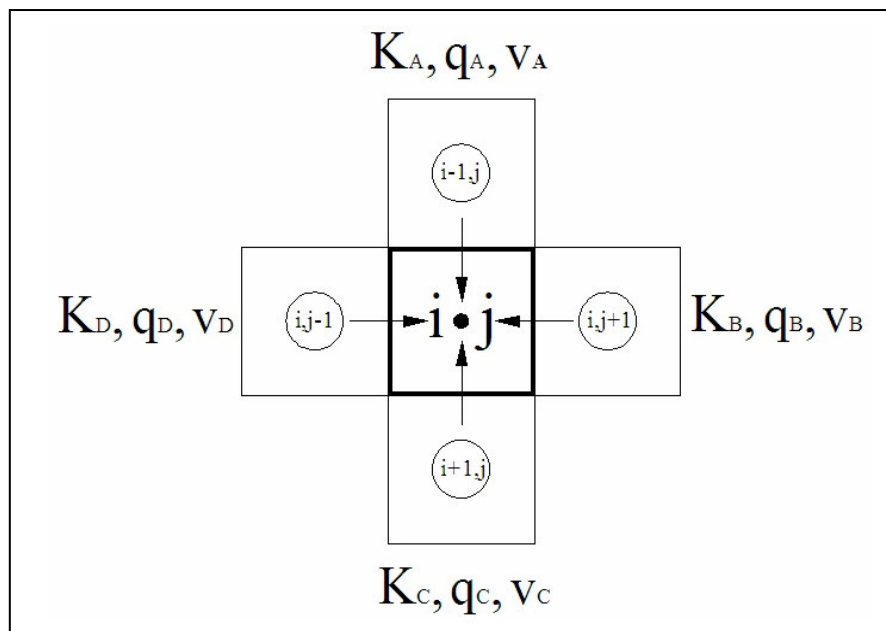
Figure 9. Example of the finite volume approach used in the computation of the hydraulic head and flow velocity at every node within the (100m x 10m) domain.

C. Groundwater Velocity

Similarly to the hydraulic head calculation, the FVM was also used to determine the groundwater flow at a certain node, as fluxes from the four adjacent nodes to the cell

in question. From Eq. 4, the four velocity vectors surrounding node (i, j) can be estimated by:

$$v_A = \frac{K_A}{n} \frac{(h_{i-1,j} - h_{i,j})}{\Delta y}; v_B = \frac{K_B}{n} \frac{(h_{i,j+1} - h_{i,j})}{\Delta x}$$

$$v_C = \frac{K_C}{n} \frac{(h_{i+1,j} - h_{i,j})}{\Delta y}; v_D = \frac{K_D}{n} \frac{(h_{i,j-1} - h_{i,j})}{\Delta x} \tag{25}$$

D. Degradation Rate Coefficient

Since the objective of this research was to determine how contaminant fate and transport in groundwater are affected by the correlation between K and α, a certain equation linking these two variables was to be proposed. Eq. 26 below was the premise, whose validity was tested based upon numerous contaminant transport simulations:

$$\ln(\alpha) = m \ln(K) + b \tag{26}$$

where "m" and "b" are the slope and intercept, respectively, of the linear correlation $\ln(\alpha)$-$\ln(K)$. In the case where K and α are positively correlated (PC), "m" would be a positive integer (m > 0); when K and α are negatively correlated (NC), "m" would be a negative integer (m < 0).

From basic probabilistic and statistical operations, multiplying a random variable (K) by a constant value (m) multiplies the expected value or mean by that same constant [*Montgomery and Hines*, 1972]. Eq. 26 becomes:

$$\text{mean}[\ln(\alpha)] = m * \text{mean}[\ln(K)] + b \tag{27}$$

Knowing that the hydraulic conductivity fields generated by the HGM have a zero mean, Eq. 27 yields:

$$\text{mean}[\ln(\alpha)] = b \tag{28}$$

Another statistical manipulation of Eq. 26 can also be performed based on the fact that multiplying a random variable (K) by a constant (m) increases the variance (var) by the square of the constant [*Montgomery and Hines*, 1972]:

$$\text{var}[\ln(\alpha)] = m^2 * \text{var}[\ln(K)] + \text{var}(b) \tag{29}$$

Since var [ln (K)] = 1 (refer to Chapter IV) and var (b) = 0 (variance of a constant is always null), it follows that var [ln (α)] = m^2. It has been assumed throughout this work that m = +1 for the PC case, and m = -1 for the NC case. Therefore, the variance of ln (α) is 1, equal to the variance of ln (K).

The total time for the contaminant plume to travel from the left boundary of the aquifer to the right boundary (L_X = 100 m) can be approximated as follows:

- Head gradient = $\nabla h = 1 / 100 = 0.01$ (from Eq. 2).

- mean [ln (K)] = 0 → $K \approx e^0 \approx 1.0$ m/d.

- $q = K * 0.01$ → $q \approx 0.01$ m/d (from Eq. 1).

- $v = q / n = 0.03$ m/d (from Eq. 4).

- Time for groundwater to move from left to right boundary:

$$t = L_X / v \approx 9 \text{ years} \tag{30}$$

In order to estimate the "b" constant in Eq. 26, we specified that the steady-state solute's concentration halfway through the aquifer ($X = 50$ m) should be approximately $C = 0.01$ mg/L. Since the contaminant was undergoing 1st order kinetics' degradation, the remaining concentration was estimated using:

$$e^{-\alpha t} = 0.01 \tag{31}$$

where t = 4.5 years is the approximate time for the solute to travel 50 m.

From Eq. 31, we get $\alpha = 0.0027$ d^{-1}, which can be plugged into Eq. 28 to obtain:

$$b \approx \ln (0.0027) \approx -5.8768 \tag{32}$$

Hence, the correlation between the aquifer's hydraulic conductivity and the solute's degradation rate can be written as follows:

$$\alpha = e^{\left[\pm \ln(K) - 5.8768\right]} \tag{33}$$

E. Contaminant Concentration

A Crank-Nicolson algorithm, coupled with a finite volume approximation (MATLAB code), was used to determine the solute's concentration values across the aquifer based on Eq. 14, which was slightly altered to account for the 2-D flow (longitudinal and transverse directions):

$$\begin{aligned}
\frac{\partial C}{\partial t} &= v_A \frac{1}{\Delta y} C_{i-1/2} + v_B \frac{1}{\Delta x} C_{j+1/2} + v_C \frac{1}{\Delta y} C_{i+1/2} + v_D \frac{1}{\Delta x} C_{j-1/2} \\
&+ D_x \frac{1}{\Delta x}\left[\left.\frac{\partial C}{\partial x}\right|_{j+1/2} - \left.\frac{\partial C}{\partial x}\right|_{j-1/2}\right] + D_y \frac{1}{\Delta y}\left[\left.\frac{\partial C}{\partial y}\right|_{i+1/2} - \left.\frac{\partial C}{\partial y}\right|_{i-1/2}\right] - \alpha C
\end{aligned} \tag{34}$$

The above PDE was transformed into ordinary differential equations (ODE) using a Taylor series approximation. The ODEs were then converted into algebraic equations (Eq. 35), whose solution was C(x, y, t).

$$\begin{aligned}
\frac{C_{i,j}^{t+\Delta t} - C_{i,j}^t}{\Delta t} &= \frac{D_x(C_{i,j+1} - 2C_{i,j} + C_{i,j-1})}{\Delta x^2} + \frac{D_y(C_{i+1,j} - 2C_{i,j} + C_{i-1,j})}{\Delta y^2} \\
&+ \frac{v_A(C_{i,j} + C_{i-1,j})}{2\Delta y} + \frac{v_B(C_{i,j} + C_{i,j+1})}{2\Delta x} + \frac{v_C(C_{i,j} + C_{i+1,j})}{2\Delta y} + \frac{v_D(C_{i,j} + C_{i,j-1})}{2\Delta x} - \alpha C_{i,j}
\end{aligned} \tag{35}$$

F. Boundary Conditions

As in any numerical model, a set of initial and boundary conditions were to be pre-specified in order to solve for the head and concentration values throughout the aquifer.

It has already been stated in preceding sections that head values were set to be constant on both the left (j = 1) and right (j = N) boundaries (Figure 6). Furthermore, it was assumed that at the left boundary, a constant contaminant concentration C_o = 100 mg/L was to be maintained at all times. No longitudinal dispersive flux was allowed at the right boundary. Both top and bottom layers were set as no-flow boundaries (no advective flux; no transverse dispersive flux).
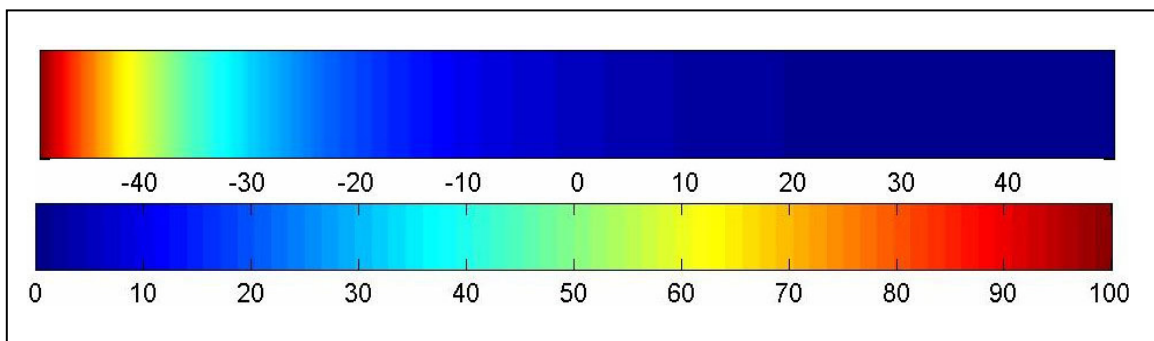
Figure 10. Concentration profile along a (100m x 10m) aquifer having a uniform hydraulic conductivity and degradation rate (K = 1.0 m/d, α = 0.0027 d^{-1}).

CHAPTER V

RESULTS

As described in the previous section, the aquifer's parameters listed in Table 1 along with the boundary conditions were all included in a MATLAB algorithm, which was used to compute the reactive solute's concentration values at the center of all cells within the (100m x 10m) aquifer. For each of the 50 hydraulic conductivity fields illustrated in Table 3, two transport simulations were conducted: the first one corresponding to K and α being positively correlated (Eq. 36), and the second one for K and α being negatively correlated (Eq. 37).

$$\alpha_{i,j} = e^{\left[+\ln(K_{i,j})-5.8768\right]} \tag{36}$$

$$\alpha_{i,j} = e^{\left[-\ln(K_{i,j})-5.8768\right]} \tag{37}$$

Since it has been shown that $t = 9$ years was an approximate time interval for the contaminant to migrate from one side of the aquifer to the other (Eq. 30), each simulation was carried out for a period $T = 15$ years to ensure sufficient time for the concentration profile to reach steady-state. Comparison of simulations using $T = 15$ years and $T = 20$ years verified that steady state was reached within 15 years.

A. Qualitative Analysis

In each of the Figures 11 through 16 below, three graphs are presented: the top graph represents the normally distributed ln (K) field generated using the HGM; the middle and bottom graphs correspond to the contaminant's concentration profiles along the aquifer for the PC (m = +1) and NC (m = -1) cases, respectively. All profiles are shown at T = 15 years, at which point the concentration profiles have reached steady state.
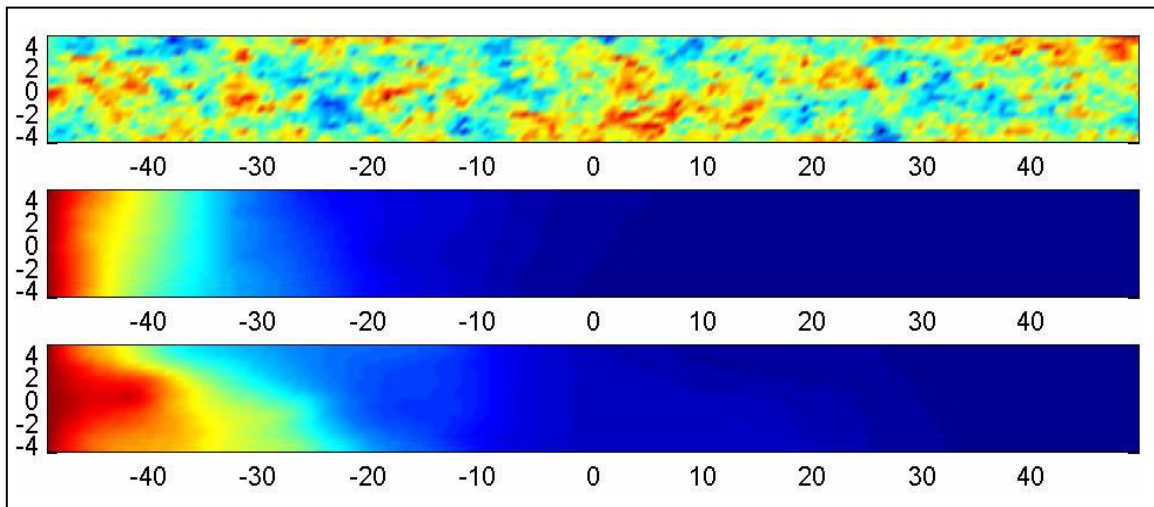
Figure 11. Concentration profiles for the PC and NC cases based on the hydraulic conductivity values from replicate 11 (Table 3).
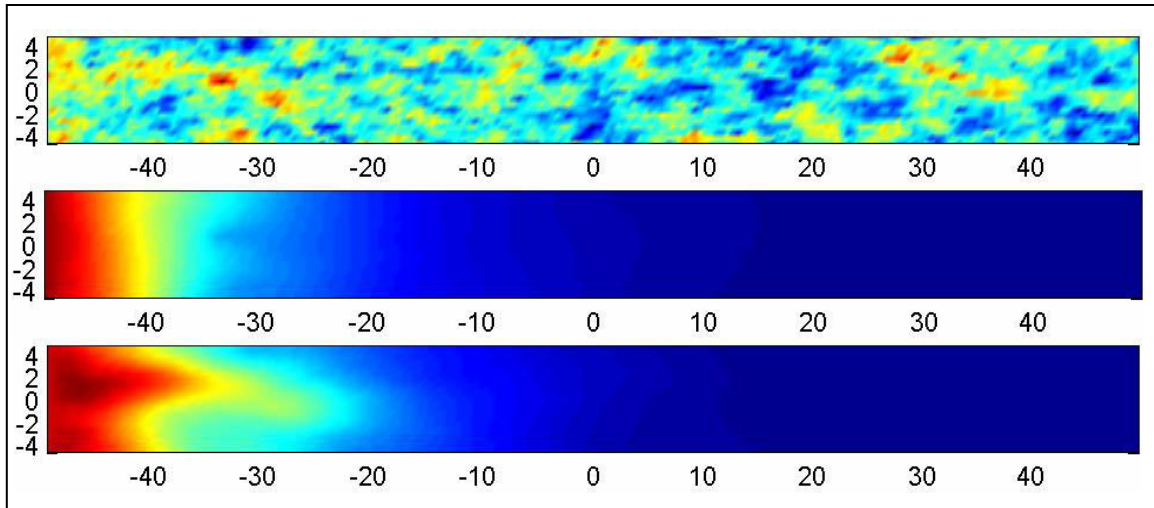
Figure 12. Concentration profiles for the PC and NC cases based on the hydraulic conductivity values from replicate 6 (Table 3).
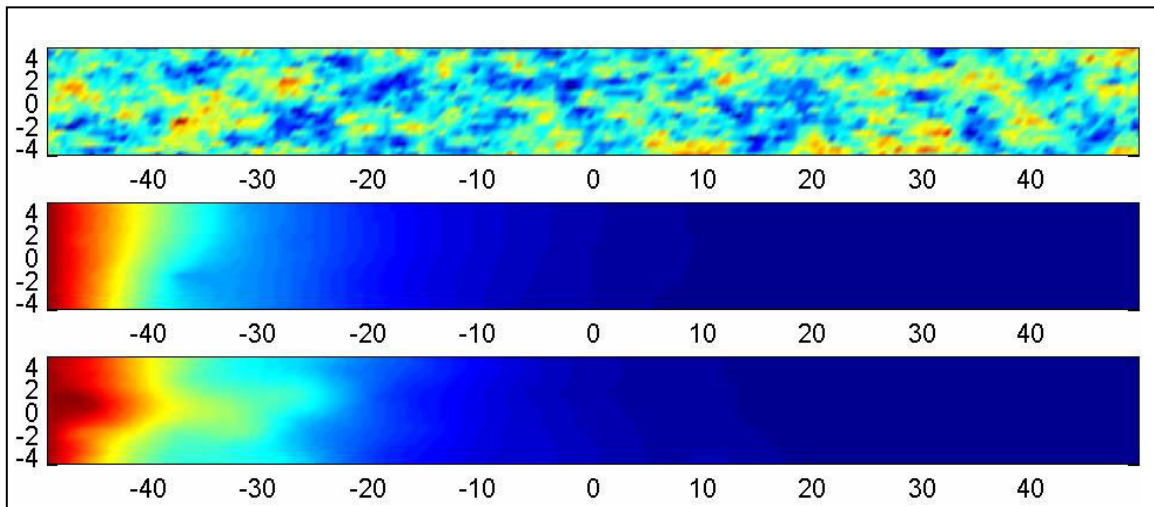
Figure 13. Concentration profiles for the PC and NC cases based on the hydraulic conductivity values from replicate 2 (Table 3).

From a qualitative point of view, the PC cases in Figures 11, 12, and 13 look rather uniform, as if the solute was moving in a homogeneous environment (refer to Figure 10). The NC cases exhibit more fingering and the contamination front is more advanced in the direction of the domain's right boundary. A larger hydraulic conductivity variance (var [K] ≈ 1 in this work) would have probably led to more extreme fingering of the contaminated plume.
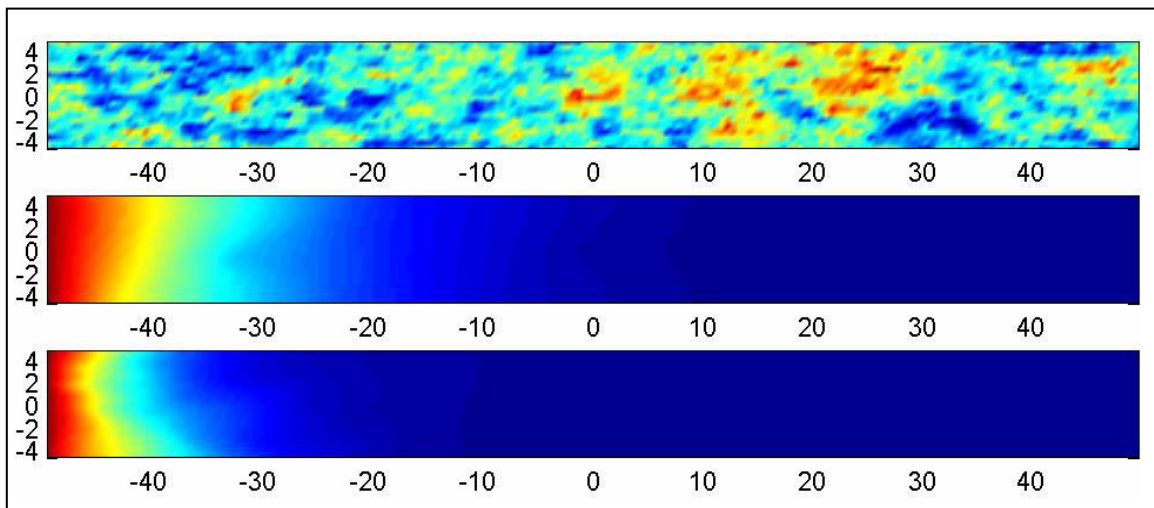
Figure 14. Concentration profiles for the PC and NC cases based on the hydraulic conductivity values from replicate 15 (Table 3).
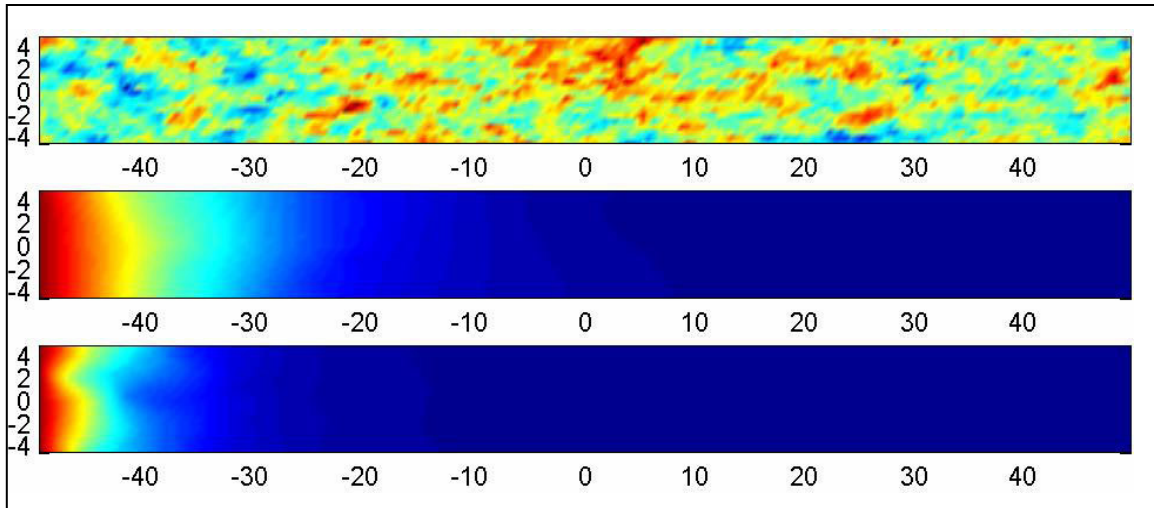
Figure 15. Concentration profiles for the PC and NC cases based on the hydraulic conductivity values from replicate 42 (Table 3).
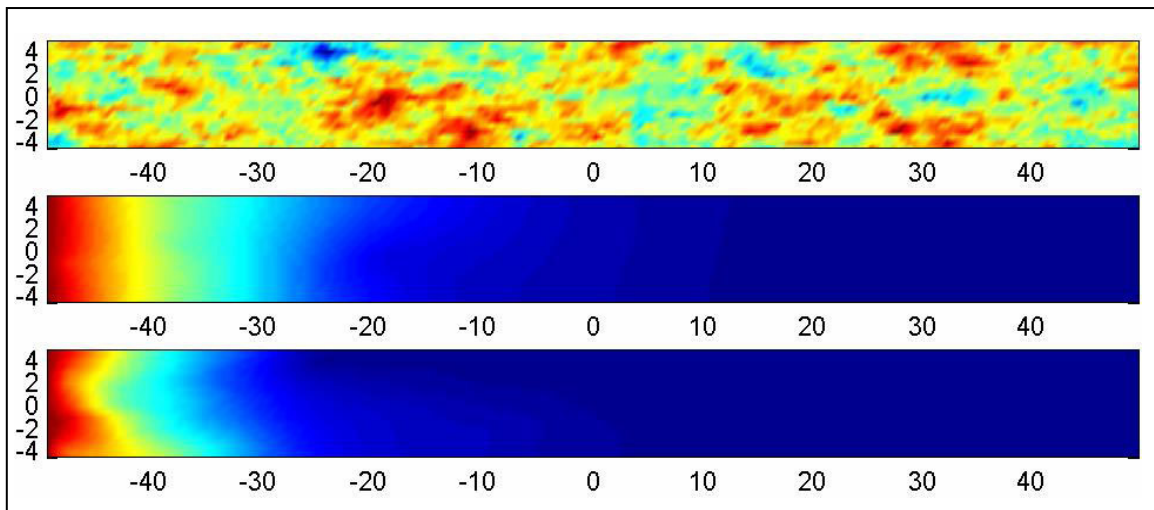
Figure 16. Concentration profiles for the PC and NC cases based on the hydraulic conductivity values from replicate 29 (Table 3).

Figures 14, 15, and 16 display quite the opposite effects from those previously described (11 - 12 - 13). The PC graphs show more spreading of the contamination front, which remains closer to the left boundary in the NC profiles. It is worth noting, though, that the PC graphs still appear to be more uniformly distributed. This is probably due to the fact that, in the PC case, more degradation occurs in the highly transmissive regions (having high K) where solutes can spread more easily. Whereas in the NC case, regions having high hydraulic conductivity values reflect relatively low degradation levels, which might explain the fingering and random behavior of the contaminated plume.

B. Quantitative Analysis

In order to quantify the difference in the solute's behavior in both cases, a spatial moments' analysis was adopted to provide a more integrated measure of the contaminated plume's distribution [*Yeh et al.*, 1995]. The zeroth spatial moment, M_{00}, represents the total mass of solute remaining within the rectangular domain. The center of mass (centroid) of the contaminated cloud, X_c, is determined by normalizing the first spatial moment, M_{10}, by the total remaining mass.

$$M_{00} = \sum_{e=1}^{E} nC_e(x, y, t)V_e \tag{38}$$

$$M_{10} = \sum_{e=1}^{E} nC_e(x, y, t) x_e V_e \tag{39}$$

$$X_c = \frac{M_{10}}{M_{00}} \tag{40}$$

where $C_e(x, y, t)$ is the concentration at node "e", having spatial coordinates (x, y), at time t; "E" is the total number of nodes within the domain; x_e is the abscissa at the node's center; $V_e = (\Delta x \Delta y \Delta z)$ is the node's volume (the thickness, $\Delta z = 1$ m, is assumed to constant throughout the aquifer).

Table 4. Zeroth Spatial Moment, First Spatial Moment, and Center of Mass Location (PC and NC cases) for the 50 Simulated Fields.

Replicate	PC M_{00}, kg	PC M_{10}, kg.m	PC X_c, m	NC M_{00}, kg	NC M_{10}, kg.m	NC X_c, m
1	4.19	57.99	13.86	5.51	93.53	16.96
2	4.84	70.43	14.54	6.28	104.85	16.70
3	4.98	72.27	14.51	4.62	59.81	12.95
4	5.57	78.89	14.17	5.91	86.23	14.59
5	5.75	85.70	14.91	4.43	53.47	12.07
6	5.36	81.70	15.24	7.28	120.96	16.60
7	5.29	74.01	14.00	3.56	40.74	11.43
8	4.26	58.32	13.69	3.37	42.59	12.65
9	4.70	66.86	14.22	4.16	54.95	13.20
10	4.50	65.32	14.51	6.11	97.88	16.03
11	4.50	59.42	13.21	7.05	136.27	19.32
12	4.60	61.76	13.42	5.85	99.24	16.97
13	4.26	54.57	12.81	3.99	54.88	13.74
14	3.71	47.26	12.73	4.65	85.19	18.33
15	5.48	81.72	14.92	3.16	30.17	9.56
16	4.62	69.73	15.08	5.05	75.35	14.91

Table 4   (continued)

17	5.67	83.23	14.68	4.77	58.30	12.23
18	4.15	51.17	12.34	4.01	67.14	16.73
19	5.11	75.44	14.78	5.26	77.39	14.71
20	4.56	63.23	13.85	6.90	130.50	18.92
21	6.07	87.83	14.48	7.42	117.42	15.82
22	4.07	55.67	13.68	5.49	90.85	16.55
23	4.36	60.25	13.81	6.46	108.57	16.80
24	5.40	78.90	14.61	5.06	66.60	13.16
25	4.45	56.88	12.79	2.78	27.99	10.05
26	4.12	60.67	14.72	5.91	92.46	15.65
27	4.92	70.99	14.42	4.96	70.44	14.21
28	4.86	64.96	13.38	4.37	63.54	14.55
29	5.39	81.85	15.17	3.75	40.63	10.84
30	4.65	61.16	13.15	4.48	66.52	14.85
31	5.99	92.52	15.45	4.52	52.84	11.68
32	4.02	49.32	12.27	4.37	72.01	16.46
33	4.53	60.09	13.27	5.24	87.16	16.63
34	4.44	58.88	13.26	5.83	102.03	17.50
35	5.32	76.41	14.36	5.31	74.83	14.09
36	5.04	73.51	14.58	7.72	138.55	17.95
37	4.97	72.58	14.59	4.99	72.07	14.43
38	4.73	64.34	13.61	4.76	73.11	15.36
39	5.06	71.47	14.11	5.44	84.40	15.51
40	4.71	63.37	13.46	3.70	46.22	12.50
41	4.05	50.65	12.52	5.66	104.71	18.49
42	5.00	69.23	13.84	2.53	22.03	8.70
43	4.60	64.26	13.97	4.20	55.27	13.17
44	4.78	67.24	14.07	5.32	78.56	14.76
45	5.34	75.03	14.04	9.29	180.84	19.46
46	4.66	64.22	13.77	4.15	52.76	12.71
47	5.13	77.90	15.19	4.40	56.14	12.76
48	4.63	65.92	14.23	5.94	97.13	16.35
49	4.44	58.96	13.28	4.88	75.52	15.46
50	4.26	54.01	12.69	5.83	112.11	19.23

One important parameter that plays a role in characterizing the solute's behavior in both the PC and NC cases is the contaminated plume's travel distance. $X_{1\%}$ is the abscissa of the point beyond which the solute's concentration is less than 1% of its initial inlet concentration (C_o = 100 mg/L). In other words, $X_{1\%}$ represents the maximum distance traveled by the contamination. It can be considered as a measure of the plume's fingering. ($X_{1\%}$ - X_c) can also be regarded as another factor that describes the extent of the plume's spread along the aquifer. Note that X_c and $X_{1\%}$ vary between 0 and 100, corresponding to -50 and 50, respectively in the concentration profiles.

Table 5. Contaminated Plume's Travel Distance for the 50 Simulated Fields (PC and NC cases).

Replicate	P C		N C	
	$X_{1\%}$, m	($X_{1\%}$ - X_c), m	$X_{1\%}$, m	($X_{1\%}$ - X_c), m
1	64.50	50.65	85.00	68.04
2	66.00	51.46	85.50	68.80
3	66.00	51.49	63.00	50.05
4	68.00	53.83	76.00	61.41
5	71.00	56.09	57.50	45.43
6	71.50	56.26	71.00	54.40
7	67.00	53.00	61.00	49.57
8	62.00	48.31	60.50	47.85
9	66.50	52.28	67.50	54.30
10	68.00	53.49	68.50	52.47
11	61.50	48.29	100.00	80.68
12	66.00	52.58	91.50	74.53
13	60.50	47.69	69.50	55.76
14	59.00	46.27	83.00	64.67
15	65.00	50.08	44.00	34.44
16	67.00	51.92	66.50	51.59
17	68.00	53.32	67.50	55.27

Table 5   (continued)

18	63.50	51.16	76.00	59.27
19	69.00	54.22	64.00	49.29
20	64.50	50.65	93.00	74.08
21	67.50	53.02	87.50	71.68
22	65.00	51.32	68.00	51.45
23	61.50	47.69	79.00	62.20
24	69.00	54.39	63.50	50.34
25	60.50	47.71	50.50	40.45
26	67.50	52.78	65.00	49.35
27	65.50	51.08	66.50	52.30
28	62.50	49.12	76.50	61.95
29	69.00	53.83	55.50	44.66
30	64.00	50.85	79.00	64.15
31	74.00	58.55	58.50	46.82
32	60.50	48.23	81.50	65.04
33	62.50	49.23	78.00	61.37
34	63.50	50.24	78.50	61.00
35	61.50	47.14	73.00	58.91
36	69.50	54.92	85.00	67.05
37	68.50	53.91	76.50	62.07
38	66.50	52.89	76.50	61.14
39	68.00	53.89	78.50	62.99
40	64.50	51.04	63.50	51.00
41	61.50	48.98	86.50	68.01
42	67.00	53.16	44.00	35.30
43	65.00	51.03	72.00	58.83
44	63.50	49.43	63.50	48.74
45	71.50	57.46	82.00	62.54
46	62.50	48.73	61.50	48.79
47	66.50	51.31	59.00	46.24
48	69.50	55.27	66.50	50.15
49	63.00	49.72	77.50	62.04
50	57.50	44.81	89.00	69.77

Table 6. Comparison of the Arithmetic Mean and Standard Deviation (STDEV) of the 50 Simulated Fields (PC and NC cases).

	P C			N C		
	M_{00}, kg	X_c, m	$X_{1\%}$, m	M_{00}, kg	X_c, m	$X_{1\%}$, m
Mean, μ	4.80	13.96	65.46	5.13	14.89	71.85
STDEV, σ^2	0.54	0.81	3.51	1.31	2.60	12.22

1. Zeroth Spatial Moment

In the work by *Miralles-Wilhelm and Gelhar* [1996], the authors state that the effective decay constant is not a function of the K-α correlation. Therefore, on average, a positive or a negative correlation should both result in the same mass of solute remaining. This statement is confirmed by the findings in Table 6, where the averaged zeroth moments for the PC and NC cases are roughly equal. However, the NC cases exhibit more variability in the solute's remaining mass, which ranges from 2.5 kg to 9.3 kg, whereas M_{00} varies only between 3.7 kg and 6 kg in the PC cases (Table 4). This variability is quantified in Table 6 where, for approximately the same arithmetic mean, σ^2 in the NC cases is almost three times as large as σ^2 in the PC cases.

It can also be inferred, from Miralles-Wilhelm and Gelhar's statement, that 25 cases should have a higher M_{00} for a positive K-α correlation, and 25 cases should have a higher M_{00} for a negative correlation. In this work, 29 simulated fields have more mass remaining in the NC case, as opposed to 21 having more mass in the PC case, which

shows that the simulation results agree with the theoretical prediction despite the small discrepancy.

2. First Spatial Moment

The contaminated plume's centroid is located, on average, within a 1 m interval for both PC and NC cases (Table 6). The $X_{1\%}$ parameter is slightly higher in the NC case than in the PC case. The 10% difference in $X_{1\%}$ (71.85 – 65.46 = 5.99 m) suggests that the NC cases exhibit more fingering than the PC cases. Had var[ln(K)] been larger than 1 (Table 2), the difference in the plume's spreading might have been more discernible (higher than 10%).

Similarly to the zeroth moment analysis, the first spatial moments in the NC case display a high degree of variability (Table 4), which is again manifested by the fact that, for both $X_{1\%}$ and X_c, σ^2 in the NC cases is over three times larger than σ^2 in the PC cases (Table 6). This can only assert the conclusion drawn from the qualitative analysis, as to the relatively uniform behavior of the plume in the PC case compared to the randomness and irregularity that govern a negative K-α correlation.

3. Homogeneous vs. Heterogeneous

According to *Miralles-Wilhelm and Gelhar* [1996], the effective decay rate should be less than the mean decay rate. This implies a larger remaining mass in a heterogeneous aquifer as compared to a homogeneous case. In order to verify this statement, a transport simulation was conducted along a homogeneous domain having the same prescribed spatial statistics as those of the heterogeneous case. The arithmetic mean of the aquifer's K and α were computed as follows:

$$\text{mean} \quad (K) \quad = \quad e^{\left(\mu_{\ln (K)} + \frac{\sigma^2_{\ln (K)}}{2} \right)} \tag{41}$$

$$\text{var} \ (\alpha) = e^{\left(\mu_{\ln (\alpha)} + \frac{\sigma^2_{\ln (\alpha)}}{2} \right)} \tag{42}$$

where $\mu_{\ln(K)} = 0$ and $\sigma^2_{\ln(K)} = 1$ (Table 2); $\mu_{\ln(\alpha)} = -5.8768$ (Eq. 38) and $\sigma^2_{\ln(\alpha)} = 1$ (Eq. 29).

For K = 1.65 m/d, $\alpha = 0.00462$ d^{-1}, and with all the other hydrological parameters (porosity, dispersion coefficient, etc.) used in the heterogeneous case (Table 1), the remaining mass within the homogeneous aquifer (Figure 17) was 5080 g, compared to an average of 4802 g in the case of a positive K-α correlation, and 5134 g for a negative K-α correlation.

The zeroth moments in the PC and NC cases are both relatively close (within a 4% interval) to the theoretical estimate of 5080 g, assuming a homogeneous K and α. This outcome does not agree with the analytical solution [*Miralles-Wilhelm and Gelhar*, 1996], which predicts a higher M_{00} value for a heterogeneous aquifer than for a homogeneous one. This may be due to the fact that *Miralles-Wilhelm and Gelhar* [1996] used a different approach for correlating K and α. Other possible reasons for the discrepancy might be their use of a spatially-varying dispersivity and a 3-D domain, as opposed to a constant dispersivity value and a 2-D domain in this work.
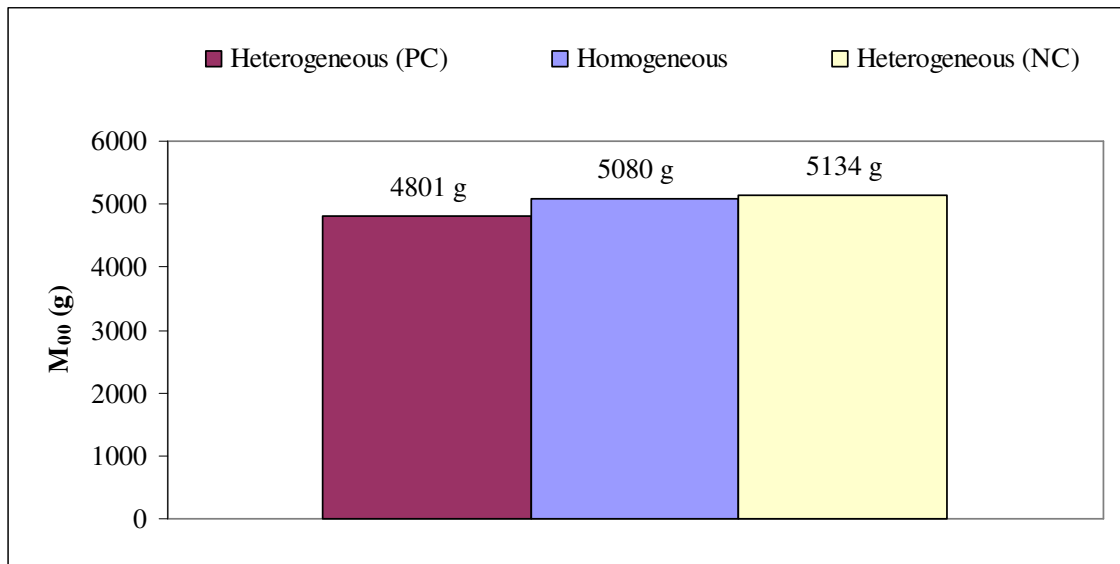
Figure 17. Comparison of the mass remaining in a homogeneous aquifer vs. a heterogeneous aquifer.

CHAPTER VI

CONCLUSIONS AND RECOMMENDATIONS

A stochastic analysis of reactive solute transport and first-order decay in two-dimensionally heterogeneous aquifers has been presented in this work. Specifically, the effects of the correlation between the spatially-variable hydraulic conductivity (K) and degradation rate (α) have been examined.

Random fields of K were generated using the HYDRO_GEN method, which has proven to be very efficient in preserving the prescribed spatial statistics (mean, variance, etc.). Two sets of transport simulations, based on a Crank-Nicolson algorithm, were conducted for 50 Monte Carlo realizations of K fields: the first set based on a positive correlation between K and α, and the second set based on a negative correlation. A spatial moments analysis has been carried out to quantify the effect of such a correlation on the contaminated plume's behavior under steady flow conditions.

It has been demonstrated that, on average, both K-α correlation scenarios lead to an equal zeroth moment (contaminant mass remaining). However, a negative correlation displayed much more variability in the mass of solute remaining within the aquifer: for roughly the same mean, the standard deviation of a negative correlation was almost three times that of a positive correlation.

Concentration profiles for positively correlated cases were marked by a relatively uniform behavior of the contaminated cloud, as opposed to a more variable spreading in the negatively correlated cases, which generally exhibited more fingering of the plume.

It has also been found that, for both cases of the K-α correlation, zeroth moments were, on average, close to those of a homogeneous aquifer. This finding has important practical implications, since it contradicts a result predicted by *Miralles-Wilhelm and Gelhar* [1996], and is hence worthy of follow-up research.

An important improvement of this study would be to investigate the K-α correlation in three-dimensional aquifers. Also, a change in the statistical characteristics (mean and variance) of the spatially-variable parameters (K, α, etc) may help clarify the effect of such a change on the contaminated plume's fingering.

In summary, the correlation between K and α has a significant influence on contaminant fate and transport in heterogeneous aquifers, including the effects demonstrated in this thesis, and is worthy of additional theoretical and experimental research.

REFERENCES

Allen-King, R. M., Halket, R. M., Gaylord, D. R., Robin, M. J. L. Characterizing the Heterogeneity and Correlation of Perchloroethene Sorption and Hydraulic Conductivity Using a Facies-Based Approach. *Water Resour. Res.*, 34(3), 385-396, 1998.

Bear, J. *Dynamics of Fluids in Porous Media*. American Elsevier, New York, 1972.

Bear, J., Verruijt, A. *Modeling Groundwater Flow and Pollution: With Computer Programs for Sample Cases*. Reidel Publishing Company, Boston, 1987.

Bellin, A., Rubin, Y. HYDRO_GEN: A Spatially Distributed Random Field Generator for Correlated Properties. *Stochastic Hydrology and Hydraulics*, 10(4), 253-278, 1996.

Benson, D.A., Wheatcraft, S.W., Meerschaert, M.M.. The Fractional-Order Governing Equation of Levy Motion. *Water Resour. Res.*, 36(6), 1413-1423, 2000.

Dagan, G. *Flow and Transport in Porous Formations.* Springer-Verlag, Berlin, 1989.

Fetter, C. W. *Applied Hydrogeology*. Prentice-Hall, Upper Saddle River, New Jersey, 1994.

Garabedian, S.P., LeBlanc, D.R., Gelhar, L.W., Celia, M.A. Large-Scale Natural Gradient Tracer Test in Sand and Gravel, Cape Cod, Massachusetts, 2, Analysis of Spatial Moments for a Nonreactive Tracer. *Water Resour. Res.*, 27(5), 911-924, 1991.

Gelhar, L. W., Axness, C. L. Three-Dimensional Stochastic Analysis of Macrodispersion in Aquifers. *Water Resour. Res.*, 19(1), 161-180, 1983.

Gelhar, L. W. *Stochastic Subsurface Hydrology*. Prentice-Hall, Englewood Cliffs, New Jersey, 1993.

Mantoglou, A., Wilson, J. L. The Turning Bands Method for Simulation of Random Fields Using Line Generation by a Spectral Method. *Water Resour. Res.*, 18(5), 1379-1394, 1982.

Matheron, J. The Intrinsic Random Functions and Their Applications. *Advances in Applied Probability*, (5), 439-468, 1973.

Mejia, J., Rodriguez-Iturbe, I. On the Synthesis of Random Fields from the Spectrum: an Application to the Generation of Hydrologic Spatial Processes. *Water Resour. Res.*, 10(4), 705-711, 1974.

Miralles-Wilhelm, F., Gelhar, L. W. Stochastic Analysis of Transport and Decay of a Solute in Heterogeneous Aquifers. *Water Resour. Res.*, 32(12), 3451-3459, 1996.

Montgomery, D., Hines, W. *Probability and Statistics in Engineering and Management Science*. The Ronald Press Company, New York, 1972.

Mood, A. F., Graybill, F. A. *Introduction to the Theory of Statistics.* McGraw-Hill, New York, 1963.

Robin, M. J. L., Sudicky, E. A., Gillham, R. W., Kachanoski, R. G. Spatial Variability of Strontium Distribution Coefficients and Their Correlation with Hydraulic Conductivity in the Canadian Forces Base Borden Aquifer. *Water Resour. Res.*, 27(10), 2619-2632, 1991.

Sudicky, E.A. A Natural Gradient Experiment on Solute Transport in a Sand Aquifer: Spatial Variability of Hydraulic Conductivity and its Role in the Dispersion Process. *Water Resour. Res.*, 22(13), 2069-2082, 1986.

Tompson, A. F. B., Gelhar, L. W. Numerical Solution of Solute Transport in Three-Dimensional, Randomly Heterogeneous Aquifer. *Water Resour. Res.*, 26(10), 2541-2562, 1990.

Yeh, T. C., Mas-Pla, J., Williams, T. M., McCarthy, J. F. Observation and Three-Dimensional Simulation of Chloride Plumes in a Sandy Aquifer Under Forced-Gradient Conditions. *Water Resour. Res.*, 31(9), 2141-2157, 1995.

APPENDIX

MATLAB ALGORITHM

```
function thesis (dx, xmax, ymax, tolerance, h_l)

% Square cells: dx = dy
% Top and bottom are no-flux boundaries: Psi_t = Psi_b = 0;
n = 0.33;
dy = dx;
h_r = h_l - 1;                              % Dh = 1 m
xmin = -xmax;
ymin = -ymax;
M = (ymax - ymin) / dx;           % M nodes in the X-direction (rows)
N = (xmax - xmin) / dx;           % N nodes in the Y-direction
(columns)

x = [xmin + 0.5*dx: dx: xmax - 0.5*dx];     % Node at center of cell
y = [ymin + 0.5*dx: dx: ymax - 0.5*dx];
[X, Y] = meshgrid (x, y);




%%%%%%%%%%%%%%%%%%%%%%%%%%%%%%%%%%%%%%%%%%%
%%            Set "k" Everywhere          %%
%%%%%%%%%%%%%%%%%%%%%%%%%%%%%%%%%%%%%%%%%%%

logk = load ('K1.txt');        % output from Hydro-Gen

for i = 1:M
    for j = 1:N
        k(i,j) = exp(logk(i,j));
    end
end

for i = 2:(M-1)
    for j = 2:(N-1)
        ka(i,j) = 2/(1/k(i-1,j) + 1/k(i,j));
        kb(i,j) = 2/(1/k(i,j+1) + 1/k(i,j));
        kc(i,j) = 2/(1/k(i+1,j) + 1/k(i,j));
        kd(i,j) = 2/(1/k(i,j-1) + 1/k(i,j));
    end
end

i = 1;
for j = 2:(N-1)
    kb(i,j) = 2/(1/k(i,j+1) + 1/k(i,j));
    kc(i,j) = 2/(1/k(i+1,j) + 1/k(i,j));
    kd(i,j) = 2/(1/k(i,j-1) + 1/k(i,j));
end
```

```
i = M;
for j = 2:(N-1)
    ka(i,j) = 2/(1/k(i-1,j) + 1/k(i,j));
    kb(i,j) = 2/(1/k(i,j+1) + 1/k(i,j));
    kd(i,j) = 2/(1/k(i,j-1) + 1/k(i,j));
end

j = N;
for i = 2:(M-1)
    ka(i,j) = 2/(1/k(i-1,j) + 1/k(i,j));
    kc(i,j) = 2/(1/k(i+1,j) + 1/k(i,j));
    kd(i,j) = 2/(1/k(i,j-1) + 1/k(i,j));
end

j = 1;
for i = 2:(M-1)
    ka(i,j) = 2/(1/k(i-1,j) + 1/k(i,j));
    kb(i,j) = 2/(1/k(i,j+1) + 1/k(i,j));
    kc(i,j) = 2/(1/k(i+1,j) + 1/k(i,j));
end

i = 1;
j = 1;
kb(i,j) = 2/(1/k(i,j+1) + 1/k(i,j));
kc(i,j) = 2/(1/k(i+1,j) + 1/k(i,j));

i = M;
j = 1;
ka(i,j) = 2/(1/k(i-1,j) + 1/k(i,j));
kb(i,j) = 2/(1/k(i,j+1) + 1/k(i,j));

i = 1;
j = N;
kc(i,j) = 2/(1/k(i+1,j) + 1/k(i,j));
kd(i,j) = 2/(1/k(i,j-1) + 1/k(i,j));

i = M;
j = N;
ka(i,j) = 2/(1/k(i-1,j) + 1/k(i,j));
kd(i,j) = 2/(1/k(i,j-1) + 1/k(i,j));




%%%%%%%%%%%%%%%%%%%%%%%%%%%%%%%%%%%%%%%%%%%%%%
%%%          Calculate head "h"          %%%
%%%%%%%%%%%%%%%%%%%%%%%%%%%%%%%%%%%%%%%%%%%%%%

% Initial Guess

% Left Boundary:
j =1;
for i = 1:M
    h(i,j) = h_l;
```

```
end

% Right Boundary:
j =N;
for i = 1:M
    h(i,j) = h_r;
end

% Interior:
J_h = (h_l-h_r) / (dx*(N-1));
for i = 1:M
    for j = 2:N-1
        h(i,j) = h_l-J_h*dx*(j-1);
    end
end

% Updating Interior "h":
error = 100;
while error > tolerance
    for i = 2:(M-1)
        for j = 2:(N-1)
            h(i,j) = (ka(i,j)*h(i-
1,j)+kb(i,j)*h(i,j+1)+kc(i,j)*h(i+1,j)+kd(i,j)*h(i,j-
1))/(ka(i,j)+kb(i,j)+kc(i,j)+kd(i,j));
        end
    end

    % Updating Top Boundary "h":
    i = 1;
    for j = 2:(N-1)
        h(i,j) = (kb(i,j)*h(i,j+1)+kc(i,j)*h(i+1,j)+kd(i,j)*h(i,j-
1))/(kb(i,j)+kc(i,j)+kd(i,j));
    end

    % Updating Bottom Boundary "h":
    i = M;
    for j = 2:(N-1)
        h(i,j) = (ka(i,j)*h(i-1,j)+kb(i,j)*h(i,j+1)+kd(i,j)*h(i,j-
1))/(ka(i,j)+kb(i,j)+kd(i,j));
    end

    % Check Error:
    error = 0;
    for i = 2:(M-1)
        for j = 2:(N-1)
            error = error + abs (h(i,j)-(ka(i,j)*h(i-
1,j)+kb(i,j)*h(i,j+1)+kc(i,j)*h(i+1,j)+kd(i,j)*h(i,j-
1))/(ka(i,j)+kb(i,j)+kc(i,j)+kd(i,j)));
        end
    end
end
```

```
%%%%%%%%%%%%%%%%%%%%%%%%%%%%%%%%%%%%
%%          Calculate V's          %%
%%%%%%%%%%%%%%%%%%%%%%%%%%%%%%%%%%%%

% Avg Pore Vel = Darcy's Vel or Specific Discharge / Eff Porosity;
% V = q / n;

% Interior Nodes
for i = 2:(M-1)
    for j = 2:(N-1)
        Va(i,j) = (1/n) * ka(i,j) * (h(i-1,j)-h(i,j))/dy;
        Vb(i,j) = (1/n) * kb(i,j) * (h(i,j+1)-h(i,j))/dx;
        Vc(i,j) = (1/n) * kc(i,j) * (h(i+1,j)-h(i,j))/dy;
        Vd(i,j) = (1/n) * kd(i,j) * (h(i,j-1)-h(i,j))/dx;
    end
end

% Top Layer (Va = 0)
i = 1;
for j = 2:(N-1)
    Va(i,j) = 0;
    Vb(i,j) = (1/n) * kb(i,j) * (h(i,j+1)-h(i,j))/dx;
    Vc(i,j) = (1/n) * kc(i,j) * (h(i+1,j)-h(i,j))/dy;
    Vd(i,j) = (1/n) * kd(i,j) * (h(i,j-1)-h(i,j))/dx;
end

% Bottom Layer (Vc = 0)
i = M;
for j = 2:(N-1)
    Va(i,j) = (1/n) * ka(i,j) * (h(i-1,j)-h(i,j))/dy;
    Vb(i,j) = (1/n) * kb(i,j) * (h(i,j+1)-h(i,j))/dx;
    Vc(i,j) = 0;
    Vd(i,j) = (1/n) * kd(i,j) * (h(i,j-1)-h(i,j))/dx;
end

% Left Boundary (Vd(i,j) = Vd(i,j+1))
j = 1;
for i = 2:(M-1)
    Va(i,j) = (1/n) * ka(i,j) * (h(i-1,j)-h(i,j))/dy;
    Vb(i,j) = (1/n) * kb(i,j) * (h(i,j+1)-h(i,j))/dx;
    Vc(i,j) = (1/n) * kc(i,j) * (h(i+1,j)-h(i,j))/dy;
    Vd(i,j) = Vd(i,j+1);
end

% Right Boundary (Vb = -Vd)
j = N;
for i = 2:(M-1)
    Va(i,j) = (1/n) * ka(i,j) * (h(i-1,j)-h(i,j))/dy;
    Vc(i,j) = (1/n) * kc(i,j) * (h(i+1,j)-h(i,j))/dy;
    Vd(i,j) = (1/n) * kd(i,j) * (h(i,j-1)-h(i,j))/dx;
    Vb(i,j) = -Vd(i,j);
end

% Upper Left Corner (Va = 0; Vd(i,j) = Vd(i,j+1))
```

```
i = 1;
j = 1;
Vb(i,j) = (1/n) * kb(i,j) * (h(i,j+1)-h(i,j))/dx;
Vc(i,j) = (1/n) * kc(i,j) * (h(i+1,j)-h(i,j))/dy;
Vd(i,j) = Vd(i,j+1);

% Lower Left Corner (Vc = 0; Vd(i,j) = Vd(i,j+1))
i = M;
j = 1;
Va(i,j) = (1/n) * ka(i,j) * (h(i-1,j)-h(i,j))/dy;
Vb(i,j) = (1/n) * kb(i,j) * (h(i,j+1)-h(i,j))/dx;
Vd(i,j) = Vd(i,j+1);

% Upper Right Corner (Va = 0; Vb = - Vd)
i = 1;
j = N;
Vc(i,j) = (1/n) * kc(i,j) * (h(i+1,j)-h(i,j))/dy;
Vd(i,j) = (1/n) * kd(i,j) * (h(i,j-1)-h(i,j))/dx;
Vb(i,j) = -Vd(i,j);

% Lower Right Corner (Vc = 0; Vb = - Vd)
i = M;
j = N;
Va(i,j) = (1/n) * ka(i,j) * (h(i-1,j)-h(i,j))/dy;
Vd(i,j) = (1/n) * kd(i,j) * (h(i,j-1)-h(i,j))/dx;
Vb(i,j) = -Vd(i,j);




%%%%%%%%%%%%%%%%%%%%%%%%%%%%%%%
%%          Calculate C      %%
%%%%%%%%%%%%%%%%%%%%%%%%%%%%%%%%%

t = 0;
T = 15;                 % years
T = T * 365;            % days
Dt = 1;                 % days
Dx = 0.3;               % m2/day
Dy = 0.03;              % m2/day
Co = 100;               % mg/L


m = +1;         %K and alpha are +vely correlated
% m = -1;       %K and alpha are -vely correlated

for i = 1:M
    for j = 1:N
        alpha(i,j) = exp (m * logk(i,j) - 5.8768);
    end
end
```

```
%%%%%%%%%%%%%%%%%%%%%%%%%%%%%%%%%%%%%%%%%%%%%%%%
%             R, W, X, Y, Z (old + new)             %
%%%%%%%%%%%%%%%%%%%%%%%%%%%%%%%%%%%%%%%%%%%%%%%%

% Interior Nodes
for i = 2:(M-1)
    for j = 2:(N-1)
        R_new(i,j) = 1/Dt + Dx/dx^2 + Dy/dy^2 - 0.25*Va(i,j)/dy -
0.25*Vb(i,j)/dx - 0.25*Vc(i,j)/dy - 0.25*Vd(i,j)/dx + alpha(i,j)/2;
        W_new(i,j) = -0.5*Dx/dx^2 - 0.25*Vb(i,j)/dx;
        X_new(i,j) = -0.5*Dx/dx^2 - 0.25*Vd(i,j)/dx;
        Y_new(i,j) = -0.5*Dy/dy^2 - 0.25*Vc(i,j)/dy;
        Z_new(i,j) = -0.5*Dy/dy^2 - 0.25*Va(i,j)/dy;

        R_old(i,j) = 1/Dt - Dx/dx^2 - Dy/dy^2 + 0.25*Va(i,j)/dy +
0.25*Vb(i,j)/dx + 0.25*Vc(i,j)/dy + 0.25*Vd(i,j)/dx - alpha(i,j)/2;
        W_old(i,j) = +0.5*Dx/dx^2 + 0.25*Vb(i,j)/dx;
        X_old(i,j) = +0.5*Dx/dx^2 + 0.25*Vd(i,j)/dx;
        Y_old(i,j) = +0.5*Dy/dy^2 + 0.25*Vc(i,j)/dy;
        Z_old(i,j) = +0.5*Dy/dy^2 + 0.25*Va(i,j)/dy;

    end
end

% Top Layer
i = 1;
for j = 2:(N-1)
    R_new(i,j) = 1/Dt + Dx/dx^2 + 0.5*Dy/dy^2 - 0.25*Vb(i,j)/dx -
0.25*Vc(i,j)/dy - 0.25*Vd(i,j)/dx + alpha(i,j)/2;
    W_new(i,j) = -0.5*Dx/dx^2 - 0.25*Vb(i,j)/dx;
    X_new(i,j) = -0.5*Dx/dx^2 - 0.25*Vd(i,j)/dx;
    Y_new(i,j) = -0.5*Dy/dy^2 - 0.25*Vc(i,j)/dy;

    R_old(i,j) = 1/Dt - Dx/dx^2 - 0.5*Dy/dy^2 + 0.25*Vb(i,j)/dx +
0.25*Vc(i,j)/dy + 0.25*Vd(i,j)/dx - alpha(i,j)/2;
    W_old(i,j) = +0.5*Dx/dx^2 + 0.25*Vb(i,j)/dx;
    X_old(i,j) = +0.5*Dx/dx^2 + 0.25*Vd(i,j)/dx;
    Y_old(i,j) = +0.5*Dy/dy^2 + 0.25*Vc(i,j)/dy;
end

% Bottom Layer
i = M;
for j = 2:(N-1)
    R_new(i,j) = 1/Dt + Dx/dx^2 + 0.5*Dy/dy^2 - 0.25*Va(i,j)/dy -
0.25*Vb(i,j)/dx - 0.25*Vd(i,j)/dx + alpha(i,j)/2;
    W_new(i,j) = -0.5*Dx/dx^2 - 0.25*Vb(i,j)/dx;
    X_new(i,j) = -0.5*Dx/dx^2 - 0.25*Vd(i,j)/dx;
    Z_new(i,j) = -0.5*Dy/dy^2 - 0.25*Va(i,j)/dy;

    R_old(i,j) = 1/Dt - Dx/dx^2 - 0.5*Dy/dy^2 + 0.25*Va(i,j)/dy +
0.25*Vb(i,j)/dx + 0.25*Vd(i,j)/dx - alpha(i,j)/2;
    W_old(i,j) = +0.5*Dx/dx^2 + 0.25*Vb(i,j)/dx;
    X_old(i,j) = +0.5*Dx/dx^2 + 0.25*Vd(i,j)/dx;
    Z_old(i,j) = +0.5*Dy/dy^2 + 0.25*Va(i,j)/dy;
end
```

```
% Left Boundary + Both (Upper and Lower) Corners
% j = 1;
% C(i,j) = Co;

% Right Boundary
j = N;
for i = 2:(M-1)
    R_new(i,j) = 1/Dt + 0.5*Dx/dx^2 + Dy/dy^2 - 0.25*Va(i,j)/dy -
0.25*Vc(i,j)/dy + 0.25*Vd(i,j)/dx + alpha(i,j)/2;
    X_new(i,j) = -0.5*Dx/dx^2 - 0.25*Vd(i,j)/dx;
    Y_new(i,j) = -0.5*Dy/dy^2 - 0.25*Vc(i,j)/dy;
    Z_new(i,j) = -0.5*Dy/dy^2 - 0.25*Va(i,j)/dy;

    R_old(i,j) = 1/Dt - 0.5*Dx/dx^2 - Dy/dy^2 + 0.25*Va(i,j)/dy +
0.25*Vc(i,j)/dy - 0.25*Vd(i,j)/dx - alpha(i,j)/2;
    X_old(i,j) = +0.5*Dx/dx^2 + 0.25*Vd(i,j)/dx;
    Y_old(i,j) = +0.5*Dy/dy^2 + 0.25*Vc(i,j)/dy;
    Z_old(i,j) = +0.5*Dy/dy^2 + 0.25*Va(i,j)/dy;
end

% Upper Right Corner (Va = 0; Vb = - Vd)
i = 1;
j = N;
R_new(i,j) = 1/Dt + 0.5*Dx/dx^2 + 0.5*Dy/dy^2 - 0.25*Vc(i,j)/dy +
0.25*Vd(i,j)/dx + alpha(i,j)/2;
X_new(i,j) = -0.5*Dx/dx^2 - 0.25*Vd(i,j)/dx;
Y_new(i,j) = -0.5*Dy/dy^2 - 0.25*Vc(i,j)/dy;

R_old(i,j) = 1/Dt - 0.5*Dx/dx^2 - 0.5*Dy/dy^2 + 0.25*Vc(i,j)/dy -
0.25*Vd(i,j)/dx - alpha(i,j)/2;
X_old(i,j) = +0.5*Dx/dx^2 + 0.25*Vd(i,j)/dx;
Y_old(i,j) = +0.5*Dy/dy^2 + 0.25*Vc(i,j)/dy;

% Lower Right Corner (Vc = 0; Vb = - Vd)
i = M;
j = N;
R_new(i,j) = 1/Dt + 0.5*Dx/dx^2 + 0.5*Dy/dy^2 - 0.25*Va(i,j)/dy +
0.25*Vd(i,j)/dx + alpha(i,j)/2;
X_new(i,j) = -0.5*Dx/dx^2 - 0.25*Vd(i,j)/dx;
Z_new(i,j) = -0.5*Dy/dy^2 - 0.25*Va(i,j)/dy;

R_old(i,j) = 1/Dt - 0.5*Dx/dx^2 - 0.5*Dy/dy^2 + 0.25*Va(i,j)/dy -
0.25*Vd(i,j)/dx - alpha(i,j)/2;
X_old(i,j) = +0.5*Dx/dx^2 + 0.25*Vd(i,j)/dx;
Z_old(i,j) = +0.5*Dy/dy^2 + 0.25*Va(i,j)/dy;




%%%%%%%%%%%%%%%%%%%%%%%%%%%%%%%%%%%%%%%%%%
%           L.H.S. Matrix (A_new)        %
%%%%%%%%%%%%%%%%%%%%%%%%%%%%%%%%%%%%%%%%%%

A_new = zeros ([M*N, M*N]);
```

```
i = 1;

for j = 2:(N-1)
    row = (i-1)*N + j;
    A_new(row, row-1) = X_new(i,j);
    A_new(row, row) = R_new(i,j);
    A_new(row, row+1) = W_new(i,j);
    A_new(row, row+N) = Y_new(i,j);
end

j = N;
row = (i-1)*N + j;
A_new(row, row-1) = X_new(i,j);
A_new(row, row) = R_new(i,j);
A_new(row, row+N) = Y_new(i,j);

for i = 2:(M-1)
    for j = 2:(N-1)
        row = (i-1)*N + j;
        if (row <= N)
            A_new(row, row-1) = X_new(i,j);
            A_new(row, row) = R_new(i,j);
            A_new(row, row+1) = W_new(i,j);
            A_new(row, row+N) = Y_new(i,j);
        else
            A_new(row, row-N) = Z_new(i,j);
            A_new(row, row-1) = X_new(i,j);
            A_new(row, row) = R_new(i,j);
            A_new(row, row+1) = W_new(i,j);
            A_new(row, row+N) = Y_new(i,j);
        end
    end


    j = N;
    row = (i-1)*N + j;
    if (row <= N)
        A_new(row, row-1) = X_new(i,j);
        A_new(row, row) = R_new(i,j);
        A_new(row, row+N) = Y_new(i,j);
    else
        A_new(row, row-N) = Z_new(i,j);
        A_new(row, row-1) = X_new(i,j);
        A_new(row, row) = R_new(i,j);
        A_new(row, row+N) = Y_new(i,j);
    end
end

i = M;
for j = 2:(N-1)
    row = (i-1)*N + j;
    if (row <= N)
        A_new(row, row-1) = X_new(i,j);
```

```
            A_new(row, row) = R_new(i,j);
            A_new(row, row+1) = W_new(i,j);
        else
            A_new(row, row-N) = Z_new(i,j);
            A_new(row, row-1) = X_new(i,j);
            A_new(row, row) = R_new(i,j);
            A_new(row, row+1) = W_new(i,j);
        end
end


j = N;
row = (i-1)*N + j;
if (row <= N)
    A_new(row, row-1) = X_new(i,j);
    A_new(row, row) = R_new(i,j);
else
    A_new(row, row-N) = Z_new(i,j);
    A_new(row, row-1) = X_new(i,j);
    A_new(row, row) = R_new(i,j);
end

j = 1;
for i = 1:M
    row = (i-1)*N + j;
    A_new(row,:) = 0;
    A_new(row, row) = 1;
end

invA = inv (A_new);




%%%%%%%%%%%%%%%%%%%%%%%%%%%%%%%%%%%%%%%%
%              R.H.S. Matrix (B)        %
%%%%%%%%%%%%%%%%%%%%%%%%%%%%%%%%%%%%%%%%

% B = zeros ([M*N,1]);
C_temp = zeros ([M*N,1]);
A_old = zeros ([M*N, M*N]);

i = 1;
for j = 2:(N-1)
    row = (i-1)*N + j;
    A_old(row, row-1) = X_old(i,j);
    A_old(row, row) = R_old(i,j);
    A_old(row, row+1) = W_old(i,j);
    A_old(row, row+N) = Y_old(i,j);
end

j = N;
row = (i-1)*N + j;
A_old(row, row-1) = X_old(i,j);
A_old(row, row) = R_old(i,j);
A_old(row, row+N) = Y_old(i,j);
```

```
for i = 2:(M-1)
    for j = 2:(N-1)
        row = (i-1)*N + j;
        if (row <= N)
            A_old(row, row-1) = X_old(i,j);
            A_old(row, row) = R_old(i,j);
            A_old(row, row+1) = W_old(i,j);
            A_old(row, row+N) = Y_old(i,j);
        else
            A_old(row, row-N) = Z_old(i,j);
            A_old(row, row-1) = X_old(i,j);
            A_old(row, row) = R_old(i,j);
            A_old(row, row+1) = W_old(i,j);
            A_old(row, row+N) = Y_old(i,j);
        end
    end

    j = N;
    row = (i-1)*N + j;
    if (row <= N)
        A_old(row, row-1) = X_old(i,j);
        A_old(row, row) = R_old(i,j);
        A_old(row, row+N) = Y_old(i,j);
    else
        A_old(row, row-N) = Z_old(i,j);
        A_old(row, row-1) = X_old(i,j);
        A_old(row, row) = R_old(i,j);
        A_old(row, row+N) = Y_old(i,j);
    end
end

i = M;
for j = 2:(N-1)
    row = (i-1)*N + j;
    if (row <= N)
        A_old(row, row-1) = X_old(i,j);
        A_old(row, row) = R_old(i,j);
        A_old(row, row+1) = W_old(i,j);
    else
        A_old(row, row-N) = Z_old(i,j);
        A_old(row, row-1) = X_old(i,j);
        A_old(row, row) = R_old(i,j);
        A_old(row, row+1) = W_old(i,j);
    end
end

j = N;
row = (i-1)*N + j;
if (row <= N)
    A_old(row, row-1) = X_old(i,j);
    A_old(row, row) = R_old(i,j);
else
    A_old(row, row-N) = Z_old(i,j);
```

```
    A_old(row, row-1) = X_old(i,j);
    A_old(row, row) = R_old(i,j);
end

j = 1;
for i = 1:M
    row = (i-1)*N + j;
    A_old(row,:) = 0;
    A_old(row, row) = 1;
end

for c = 1:(M*N)
    if rem (c,N) == 1
        C_temp (c,1) = Co;
    end
end

%%%%%%%%%%%%%%%%%%%%%%%%%%%%%%%%%%%%%%%%%%%
%           Main time-marching loop        %
%%%%%%%%%%%%%%%%%%%%%%%%%%%%%%%%%%%%%%%%%%%
while t <= T
    B = A_old * C_temp;
    C_new = invA * B;
    C_temp = C_new;
    t = t + Dt;
end

for row = 1:(M*N)
    if rem (row,N) == 1
        i = (row - 1 + N) / N;
        for z = 0:(N-1)
            J(i,1+z) = C_temp(row+z,1);
        end
    else
    end
end

%%%%%%%%%%%%%%%%%%%%%%%%%%%%%%%%%%%%%%%%%%%%%%%
%           Save Concentration Matrix J         %
%%%%%%%%%%%%%%%%%%%%%%%%%%%%%%%%%%%%%%%%%%%%%%%

save +1.txt J -ascii


figure (1);
pcolor (X, Y, J);
shading interp
axis equal tight;
hold off;

end
```

VITA

Ziad Joseph Fadel was born in Naccache, Lebanon on July 05, 1981. He received the degree of Bachelor of Engineering in Civil and Environmental Engineering at the American University of Beirut in June of 2003.

Immediately after graduation, he continued his studies in the Department of Civil Engineering at Texas A&M University and graduated with his masters in May 2005. His main interests of study are groundwater contamination and transport.

Mailing Address: 2521 Big Spring Drive

Fort Worth, TX 76120

The typist for this thesis was Ziad J. Fadel.